Politecnico di Torino

Dipartimento di Ingegneria Meccanica e Aerospaziale

Master's Degree in Biomedical Engineering
Bionanotechnologies


Politecnico
di Torino


Master's Degree Thesis

# Optimization and validation of a mechanical stimulation system for pathological *in vitro* models of cardiac tissue

**Supervisors**

Prof. Chiono Valeria

Prof. Carmagnola Irene

Doc. Spedicati Mattia

**Tutors**

Dr. Stenzig Justus

Dr. Hirt Marc

**Candidate**

Cossetta Francesca

Academic Year 2022/2023

# Abstract

Cardiovascular diseases (CVD) refer to diseases affecting the heart and blood vessels, and they pose a significant health challenge with substantial morbidity and mortality on a global scale[1]. It is important to note that CVDs are the leading cause of death worldwide[2]. At the same time, the process of discovering and developing drugs is a challenging one, and current methods for evaluating drug safety and efficacy are both costly and inefficient[3]: only 13.8% of drugs make it into phase I trials[4]. One of the fundamental factors contributing to this challenge is the limited predictive accuracy of commonly employed preclinical research models: *in vivo* animal models[5]. In addition, the choice of animal model should be carefully considered because it affects the experimental results and the ability of the study results to be translated into humans[6]. Finally, it is important to consider the ethical implications of using animal models[7]. In this context, the development of *in vitro* cardiac models that best represent the pathological conditions in humans is essential[8].
To achieve this, a system was developed to apply circular mechanical strain to engineered heart tissues (EHTs), an *in vitro* model obtained by seeding cardiomyocytes in a hydrogel and using two flexible silicone posts as support. The use of this device is advantageous for replicating pathological conditions such as those related to the cardiac preload phase and heart rate abnormalities, such as atrial fibrillation. The device can fit inside a standard cell culture incubator and all parts can be custom made using 3D printing as manufacturing technique. Furthermore, EHT technology and usage of standard 24 well plates, allow to replicate the same conditions on 24 samples simultaneously. In this work, the device design and function was optimized to obtain greater stability and a more homogeneous deformation of all support structures in all positions of a respective multi well plate. After that, an analysis method was developed using MATLAB to evaluate the stretching percentage for each well. The method allows for the analysis of videos of the flexible stretched support structure recorded during stimulation. In the final phase of the project, cellular tests were performed. Human EHTs were produced and stretched for 7 days and the force produced by them was quantified with a video-based optical analysis. After 7 days of stimulation, the culture media was analyzed to assess the presence of specific peptides produced by cells in case of heart stress, volume-related issues and myocardial damage.

# Table of contents

# 1 Introduction

## 1.1 Cardiovascular system

Blood, blood vessels, the heart, and the lymphatic system are the primary components that make up the cardiovascular system[9] (Fig. 1.1). All these elements work together to regulate the circulation in response to the needs of organs and tissues. The cardiovascular system is responsible for supplying blood to the whole body. It has the ability to control the speed and amount of blood transported through the vessels, responding to various stimuli[10]. The complex network of arteries, capillaries and veins allows the maintenance of cellular functions, the absorption of nutrients and the removal of cellular and metabolic waste[11].

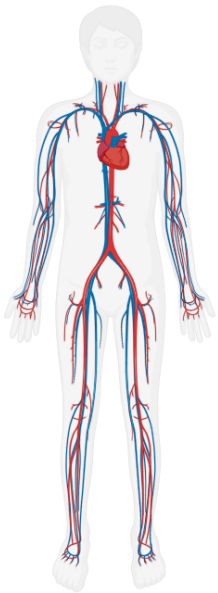

**Figure 1.1:** General view of the cardiovascular system (Created with BioRender.com).

The heart, acting as central pump, generates a pressure gradient that propels the blood, ensuring a delicate balance between arterial and venous circulation[12].

### 1.1.1 The heart

#### ANATOMY

The human heart, located in the center of the thoracic cavity, plays a fundamental role in maintaining blood flow. It is divided into four chambers: left and right atria and left and right ventricles, with the inter-ventricular septum separating them[13] (Fig. 1.2). The right side of the heart receives venous blood from the body and pump it to the lungs. After that, oxygenated blood is sent to the left side of the heart to be pumped to the whole body[14]. The upper chambers, or atria, function as receiving chambers and contract to propel blood into the lower chambers, the right ventricle and the left ventricle. The ventricles function as the main pumping chambers of the heart, pushing blood either to the lungs or to the rest of the body[15]. The atria and ventricles are separated from the mitral and tricuspid valves in the heart, while the aortic and semilunar pulmonary valves separate the ventricles from the large arteries. They are essential for preserving unidirectional blood flow and hemodynamics[16]. The presence of various cell types in the heart allows it to pump blood. They enable the generation and the transmission of electrical stimuli, which permits the required force to develop.

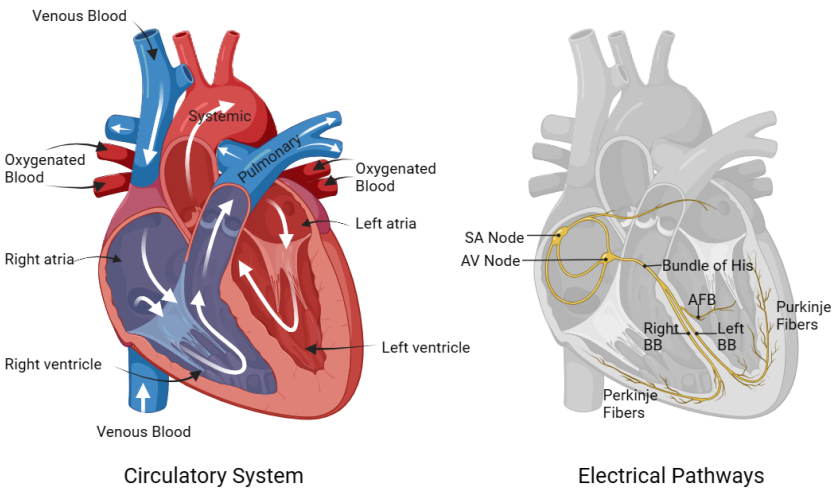


**Figure 1.2:** Anatomy and nerve structure of the heart (Created with BioRender.com).

#### CARDIAC TISSUE

The heart wall consists of three layers: the epicardium, the myocardium, and the endocardium. The myocardium is the dominant layer of striated muscle in the heart, comprising cardiac muscle cells or myocytes organized in interlocking bundles[17].

In adult cardiac tissue, various cellular elements and components of the extracel-

lular matrix (ECM) are organized in an aligned structure, collectively conferring distinctive electrical and mechanical characteristics to the tissue, enabling the flexible matrix to facilitate the circulation of blood throughout the body[18].
A multitude of cell types are present in the myocardium, including cardiomyocytes (CMs), fibroblasts (FBs), endothelial cells (ECs), pericytes, smooth muscle cells (SMCs), immune cells (myeloid and lymphoid), adipocytes, mesothelial cells, and neuronal cells[19].
To maintain a normal cardiac rhythm, it is essential for ion channels and transporters to work in coordination, enabling the orderly generation and propagation of electrical impulses across the myocardium[20]. Gap junctions, specialized protein channels in the heart, allow the transfer of ions and molecules between cells, which is essential for the heart's electrical activation. They are fundamental for the synchronized electrical function of the heart[21].

**Cardiomyocytes.** In order to ensure adequate blood perfusion, CMs within the heart must contract in a synchronized manner to perform the pump action[22]. CMs are both mechanically and electrically interconnected. These cells contain contractile units referred to as sarcomeres, composed of myosin motors and actin filaments (Fig. 1.3). These muscle fibers are organized into more extensive structures called myofibrils, forming the aligned structure of the myocardium (Fig. 1.3). Electrical signals subsequently propagate through these structures to synchronize the contraction of the heart chambers[21].

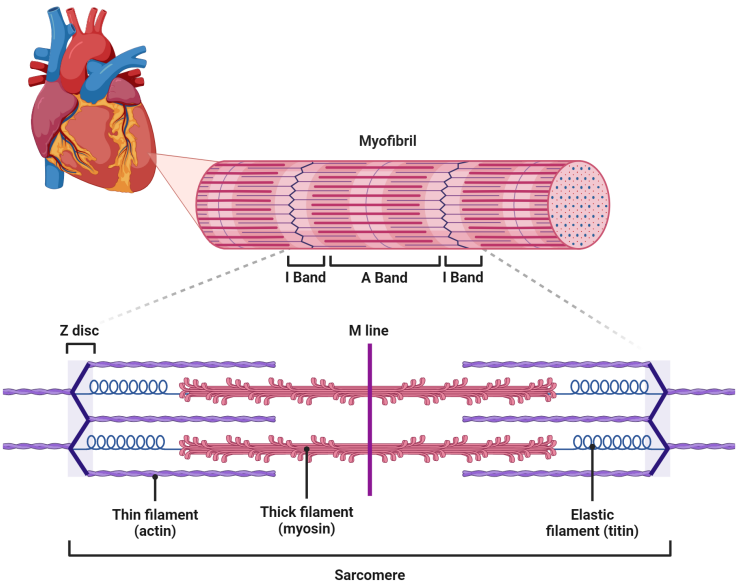


**Figure 1.3:** Structure and organization of cardiac tissue, in particular of CMs (Created with BioRender.com).

**Extracellular Matrix.** ECM components play essential roles in development, remodelling and signaling in the cardiovascular system[18]. Fibrillar collagen, elastin, and proteoglycans play vital mechanical roles in various body tissues, particularly in the cardiovascular system, while proper scar formation after myocardial infarction depends on a crucial balance between myofibroblast-mediated ECM synthesis and MMP-regulated ECM degradation[18,23].

### CARDIAC CYCLE

The sympathetic, parasympathetic, and sensory nervous systems compose the autonomic nervous system, which controls the electrical and mechanical functions of the heart[24]. The heart is equipped with a tissue able to generate and conduct the electrical impulse. The signal is conducted from the atria to the ventricular body by the bundle of His and the Purkinje fibers. These structures ensure the contraction of the heart to pump the blood to the whole body (Fig. 1.2).

Everything that happens between the beginning of one heartbeat and the beginning of the next is called the cardiac cycle. It is divided into two phases: diastole, relaxation period, and systole, contraction period[25] (Fig. 1.4). During diastole, blood from the body and lungs fills the right and left atria. Later, during the atrial systole, blood is pushed into the ventricles which, during the ventricular systole, pump blood to the body and lungs.

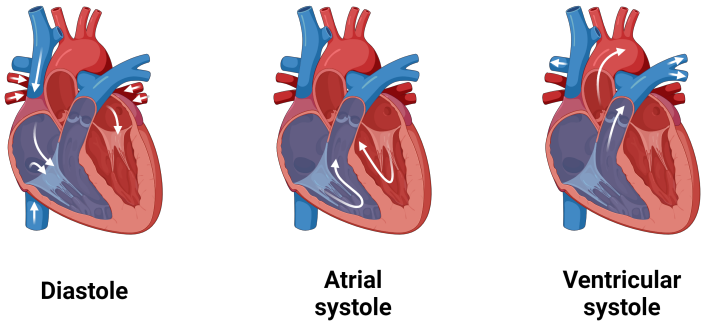


**Figure 1.4:** Illustration of the cardiac cycle that includes relaxation (diastole) and contraction (systole) of the heart, with blood flow for each phase (Created with BioRender.com).

### MECHANICAL PROPERTIES

The primary factor influencing passive myocardial stiffness and playing a crucial role in sarcomere mechanics is the collagen-rich ECM protein. Another important element is titin, an enormous protein within the cell that functions like a modifiable spring to actively regulate passive myocardial stiffness[26].

## 1.2 Cardiovascular Disease

Cardiovascular disease (CVD) is the leading cause of death in the developed as well as in the developing world[27]. CVD is categorized by a variety of disorders, which include diseases of the cardiac muscle and the vascular system that supplies the heart, brain, and other vital organs[28].

### 1.2.1 Overview

The diseases classified as CVDs include e.g. coronary heart disease, cerebrovascular disease, peripheral arterial disease, rheumatic heart disease, deep vein thrombosis and pulmonary embolism[27]. The most common CVDs are shown in the Table 1.1.

| | |
|---|---|
| **Coronary heart disease** | The myocardium does not receive enough blood or oxygen. This results from the development of an atherosclerotic plaque within the vessel's lumen.[29]. |
| **Cerebrovascular disease** | Disruption or reduction of blood flow to the brain, causing damage to brain cells. The two main types of stroke are ischemic and hemorrhagic[30]. |
| **Congenital heart disease** | It can involve the entire structure of the heart and the surrounding blood vessels. It is the most common congenital abnormality in newborns[31,32]. |
| **Heart failure** | A condition where the heart is unable to pump sufficient blood to fulfill the body's demand[33]. |
| **Cardiomyopathy** | A variety of disorders affect the cardiac muscles, reducing the heart's ability to efficiently pump blood[34,35]. |

**Table 1.1:** Description of the most common CVDs

### 1.2.2 Epidemiology and trends

CVDs are the leading cause of death worldwide today (Fig. 1.5 - 1.6). Despite advances in research, the trend in CVD incidence is growing and annual CVD mortality is expected to reach 23.6 million by 2030[36]. In addition, as one of the most expensive medical conditions, CVD imposes a significant financial strain on healthcare systems[37].

### 1.2.3 Risk factors

Current epidemiological predictions regarding CVDs indicate that the number of people with high risk of cardiovascular disease are growing and only 2%-7% of the population have no risk at all[38]. In addition, risk factors rarely occur individually and instead tend to accumulate in individuals, interacting and increasing the total risk of CVDs[39,40].

Risk factors for CVDs can be divided into two categories: medical conditions and individual behaviour.
Medical condition:

- Hypertension: it consists of elevated blood pressure and it is one of the primary risk factors for cardiovascular diseases[41].
- Hyperlipidemia: high levels of LDL cholesterol ("bad cholesterol") and low levels of HDL cholesterol ("good cholesterol") increase the risk of atherosclerosis[42].
- Diabetes: insulin resistance and diabetes can elevate the risk of cardiovascular diseases[43].
- Obesity: excess body weight is associated with increased blood pressure, cholesterol levels, and overall risk of cardiovascular diseases[44].
- Family history of cardiovascular diseases: genetic predisposition within the family can contribute to the likelihood of developing heart diseases[45].

Individual behaviour:

- Smoking: smoking is a significant risk factor for cardiovascular diseases, as it damages arteries and increases blood pressure[46].
- Unhealthy diet: a diet rich in saturated fats, cholesterol, sodium, and sugars contributes to the development of cardiovascular diseases[47] .
- Physical inactivity: lack of physical activity is associated with obesity and hypertension, increasing the risk of heart diseases[48].
- Excessive alcohol consumption: excessive alcohol consumption can elevate blood pressure and contribute to weight gain, thereby increasing the risk of cardiovascular diseases[49].
- Chronic stress: prolonged stress can adversely affect cardiac health, contributing to hypertension and inflammation[50].

In addition, it is important to consider that in some cases a condition promotes a cascade of secondary pathologies (such as diabetes due to obesity), further increasing the risk of CVDs[44].

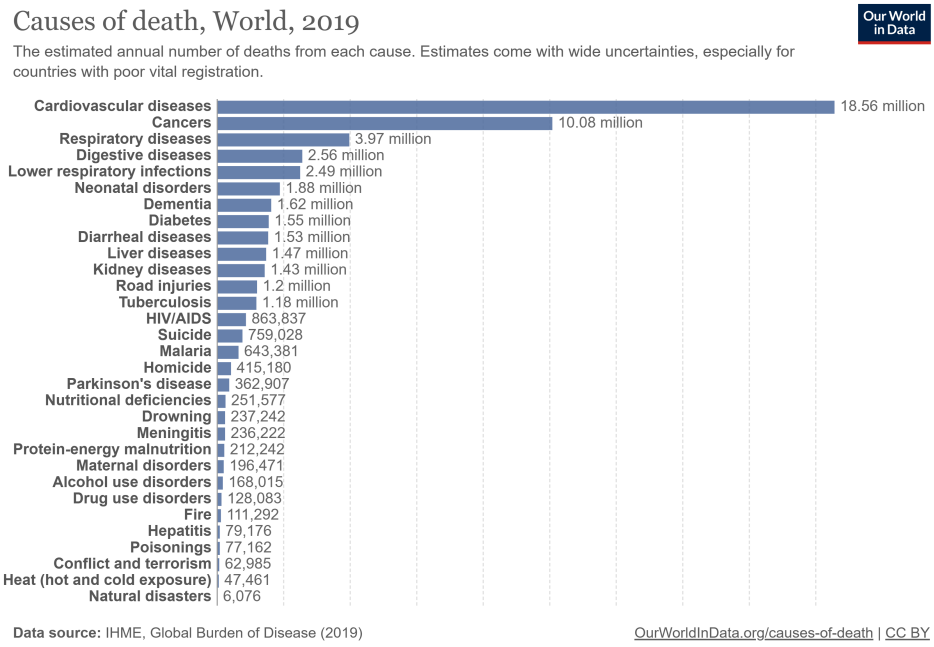


**Figure 1.5:** Causes of Death Worldwide, 2019

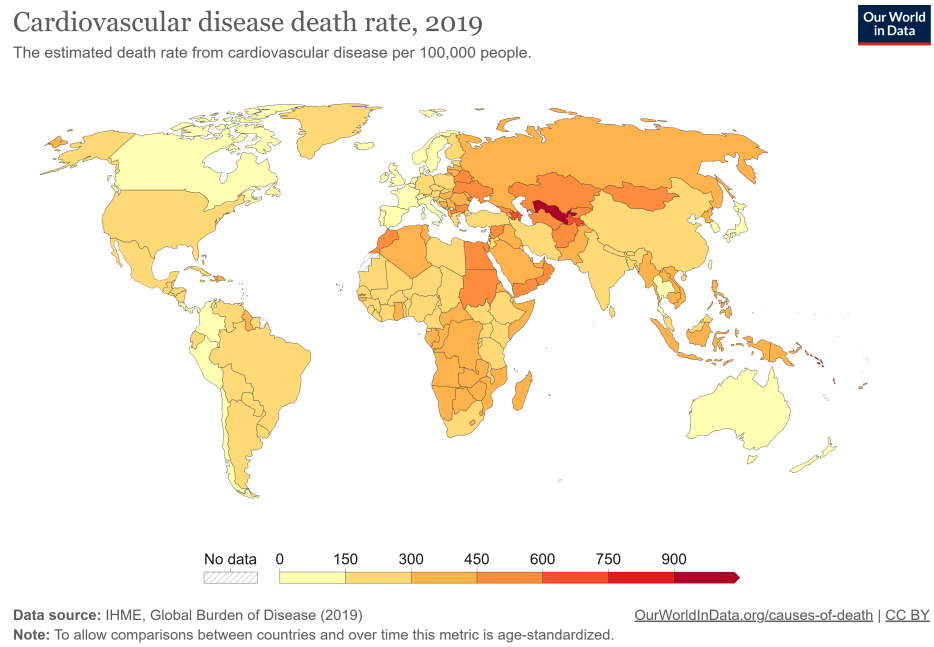


**Figure 1.6:** Deaths from Cardiovascular Diseases, 2019

## 1.3 Cardiac models

The use of CVD animal models is essential for the analysis of pathogenesis, to develop drug selection, and to test potential therapeutic strategies. Animal models that have been developed for CVD, including cardiac and atherothrombotic conditions, have given valuable insights into pathophysiology[51] . New therapeutic approaches aimed at predicting and preventing complications associated with CVD can be evaluated using these models, which have proved to be essential tools[51]. Commonly used animal models are: rats[52,53], guinea pigs[53], rabbits[53], swine[54,55], zebrafish[56,57] and dogs[54]. The choice of the animal depends on the type of research, the similarity of the physiological characteristics with those of humans and ethical considerations.

However, although animal models have been indispensable in exploring the fundamental principles of cardiogenesis, their ability to mimic the human-specific complexity of heart development, histogenesis, and physiology is remarkably limited[58] and there have been concerns about the usefulness of translating animal data to humans[59]. For example, the average rate of successful translation from animal models to clinical cancer trials is less than 8%[60].

Finally, there is an increased focus on the ethical implication of animal use[61] and compliance with 3Rs principles (Fig. 1.7), formulated by William Russell and Rex Burch. The 3Rs principles are Replacement, Reduction and Refinement and have become synonymous with measures to improve the welfare of animals used in research[62].

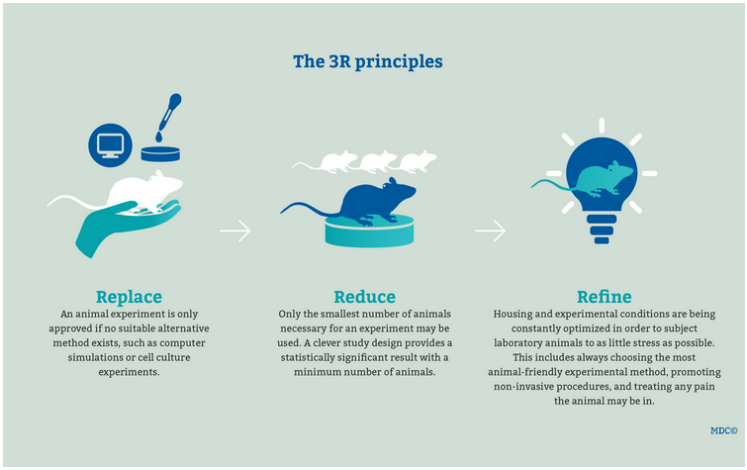


**Figure 1.7:** The 3Rs principles (https://www.mdc-berlin.de/research-animal-experiments-3r/3r-principles).

The development of *in vitro* models is necessary to reduce animal use and enhance representation of human physiology and pathologies.

### 1.3.1 *In vitro* models

The use of 2D and 3D models plays a pivotal role in scientific research, facilitating the exploration of biological processes, the assessment of efficacy of new drugs, and the advancement of sophisticated therapeutic strategies. **2D models**, such as mono-layer cell cultures, are widely employed for preliminary experiments and drug screenings, offering insights into fundamental cellular mechanisms. The investigation of complex cellular interactions and specific pathological scenarios is achievable through the use of **3D models**, such as organoids and biodegradable scaffolds, providing a more authentic representation of tissue structure. Tissue engineering research demands 3D models that closely replicate in vivo conditions.
The use of these models enables researchers to acquire detailed knowledge and manage time and resources efficiently, thereby improving understanding of diseases and developing innovative therapies.

#### 2D MODELS

**Mono-layer cell culture.** It involves growing cells on a flat surface in a uniform layer (Fig. 1.8), offering a controlled environment for studying cell proliferation, morphology, and behavior. Widely applied in toxicity testing, adhesion studies, migration experiments, gene transfection, and basic research, it helps understand cellular mechanisms[63,64].

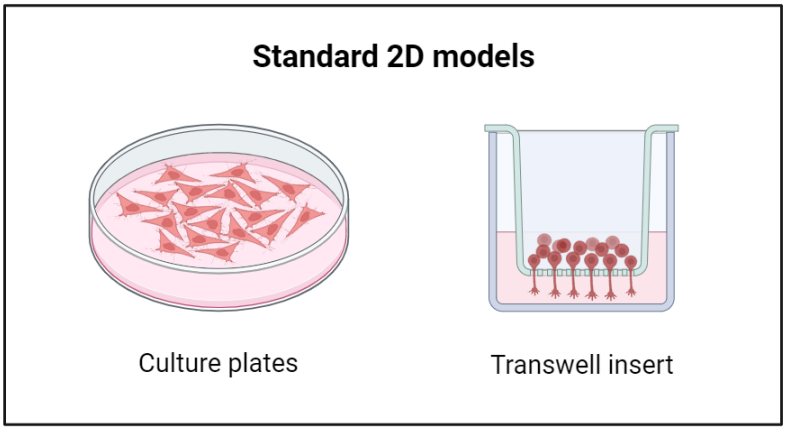


**Figure 1.8:** 2D *in vitro* models (Created with BioRender.com).

#### 3D MODELS

**Scaffold.** Crucial in 3D modeling, scaffolds provide a fundamental framework for intricate structures. Used in tissue engineering, they are vital for creating accurate 3D models, supporting diverse applications and processes in research, design, and

simulation[65,66].

**Hydrogels.** Hydrogels, hydrophilic polymer networks, are versatile materials crucial in biomedical research for drug delivery and tissue engineering. With water-absorbing properties, they mimic living tissues.[67,68] .

**Organoids.** Simple engineered tissue based on cells able to recreate different aspects of the complex structure and function of the respective tissue[69]. Crucial in disease studies, drug testing, and personalized medicine, organoids offer insights into organ-specific processes. A valuable tool for understanding complexities, they contribute to advancements in medicine and biology[69,70] .

**Organ-on-a-chip.** Organ-on-a-chip devices mimic human organ characteristics, integrating micro-fluidic channels and cultured cells. These models provide a physiologically relevant alternative for studying organ function, diseases, and drug responses. They are used for drug development and personalized medicine[71,72].

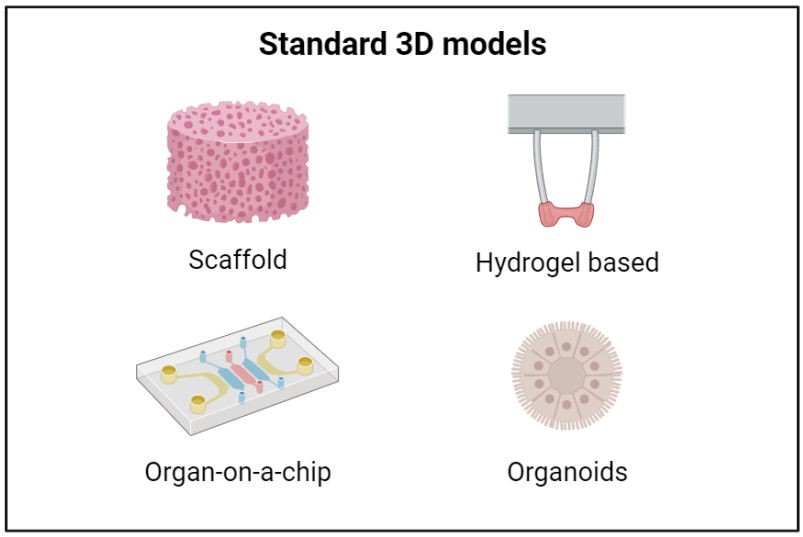


**Figure 1.9:** 3D *in vitro* models (Created with BioRender.com).

### 1.3.2 Cardiac *in vitro* models

The most common and severe adverse drug reaction in late-stage clinical development is cardiovascular toxicity caused by therapeutic drug use[73]. For this reason there is a need to develop new models to test the safety and effectiveness of drugs on the cardiovascular system. The most used *in vitro* models for drug testing are: mono-layer cell culture, hydrogels, in particular engineered heart tissue (EHT), and organ-on-a-chip. Among them, EHTs in particular are used, organizing cells within a hydrogel.

### ENGINEERED HEART TISSUE

EHTs are designed to replicate the cardiac tissue composition and function of an adult human heart by combining pre-differentiated or primary cardiac cells[58]. They are mainly made from cells embedded in hydrogel. Broadly, when high-performance toxicity screening is needed, spheroids or microtissues are chosen; when the interest concerns a model that best mimics native tissue, it is better to use heart sheets, strips, rings and chambers[4](Fig. 1.10). The primary components of EHT are hydrogel scaffolds made of bio-polymers, such as collagen or fibrin, and a sterile chamber for hydrogel culture[74].

The main cell type in the development of these models are CMs derived from induced pluripotent stem cells (iPSCs), in turn reprogrammed from somatic cells of any healthy or diseased individual. They allow to study the mechanisms of diseases in defined contexts.

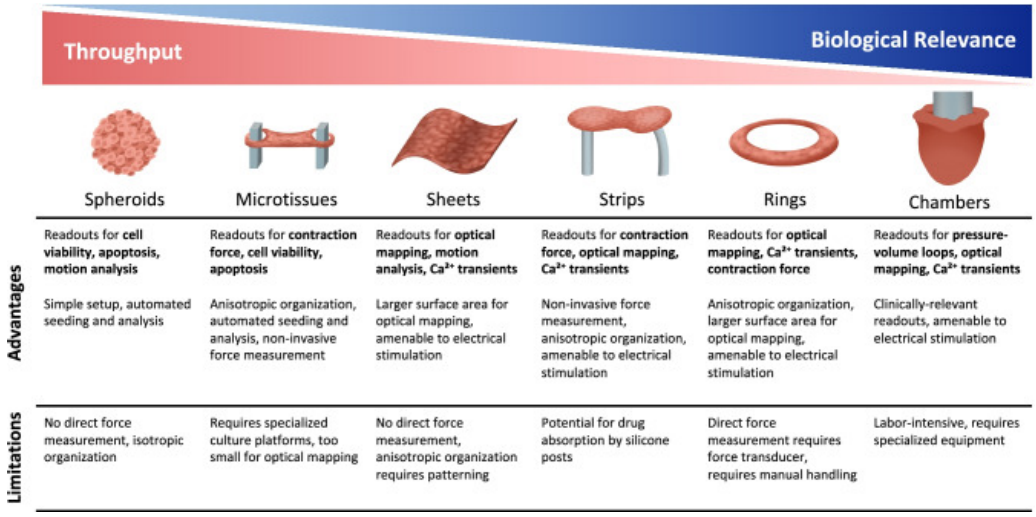


**Figure 1.10:** Different engineered cardiac tissue platforms organized by relative throughput and biological relevance with a description of their advantages and limitations[4].

## 1.4 Stimulation system

### 1.4.1 Mechanical stimulation

The aim of the project was to apply mechanical stimulation to EHTs. It has been widely shown that the application of a mechanical stimulus to heart models is useful for the development of disease models. Both atrial and ventricular myocytes subjected to mechanical stress exhibit hypertrophy[64,75].
A hypertrophic response is activated by the heart to compensate for wall stress when volume or pressure overload causes it to send stress signals[76]. The heart eventually fails as a result of progressive cardiac remodeling caused by persistent wall stress[76].
The development of an *in vitro* model representative of pathological conditions would be useful to better understand pathologies and to have a construct to test new therapies.

### 1.4.2 Previous work

The aim was the development of a device capable of replicating one or more pathological conditions for heart tissue through mechanical stimulation. It has been designed to fit into a standard cell culture incubator and all components can be produced using primarily 3D printing techniques as a production technique. The 3D heart model employed here was a miniaturized engineered heart tissue (EHT)[77].

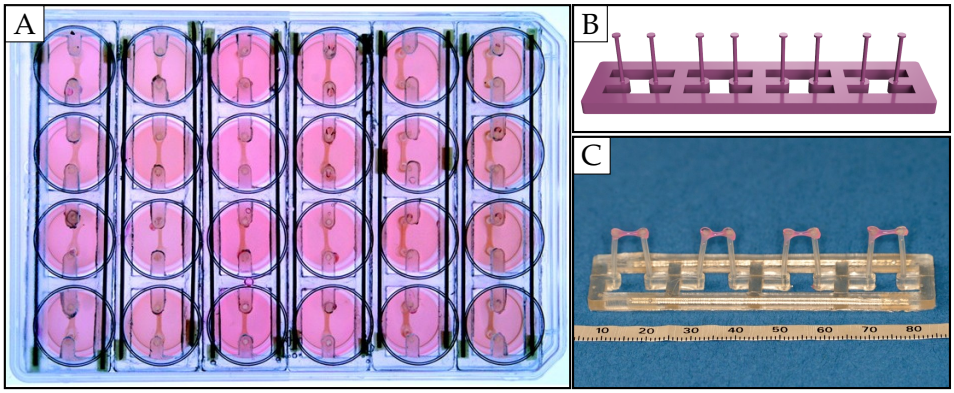


**Figure 1.11:** A) EHTs in 24-well cell culture dish, view from above; B) Rack geometry; C) Silicon post rack with four EHTs, turned upside down, scale in millimeter.

The cardiac models chosen for implementation were advantageous due to their compact size (they are cultured in standard 24-well plates) and ease of fabrication. Consequently, this allows for a high number of samples to be processed simultane-

ously and a limited use of materials.
The chosen cardiac models are created by seeding cells, suspended in a fibrin-based hydrogel, within molds containing structures with posts (Fig. 1.11B). Subsequently, through the addition of thrombin, the hydrogel polymerizes between the two posts, resulting in the model shown in Figure 1.11C after extraction from the casting molds.
The concept was to apply force at the junction between the posts and the silicone frame. This would lead to a flexion of the attachment of the posts and stretching of the EHTs (Fig. 1.12).

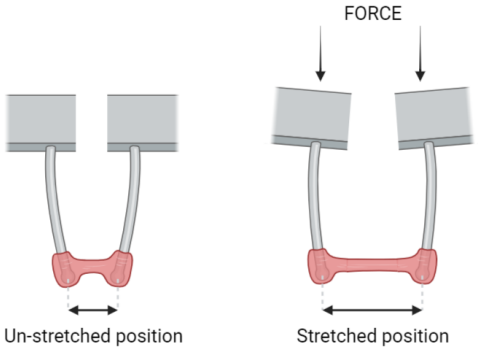


**Figure 1.12:** How the system applies force on EHTs (Created with BioRender.com).

The first version of the device had been developed by Eng. Mattia Spedicati during the practical work for his PhD thesis. The device has been designed to be used with a standard 24-well plate and to be easy to use. This includes ease of assembly and the simplicity of inserting and removing the well plate for regular media change and force analysis.
The key component to apply stretching is the grid inside the well plate, which comes into direct contact with the silicone racks.

### INTERNAL GRID

The internal grid is one of the most critical components of the system because it allows the direct application of the desired force. It consists of 48 structures, each with a hemispherical head for applying pressure to each individual post (Fig. 1.13A). In this way, each pair of posts to which each EHT is attached is stimulated, resulting in the stretching of the tissues.
After placing the internal grid, the well plate is closed with its original lid, thereby maintaining sterility (Fig. 1.13B).
The displacement of posts and consequent stimulation of EHTs is obtained by applying linear force in a rhythmic manner directly to the well plate cover.

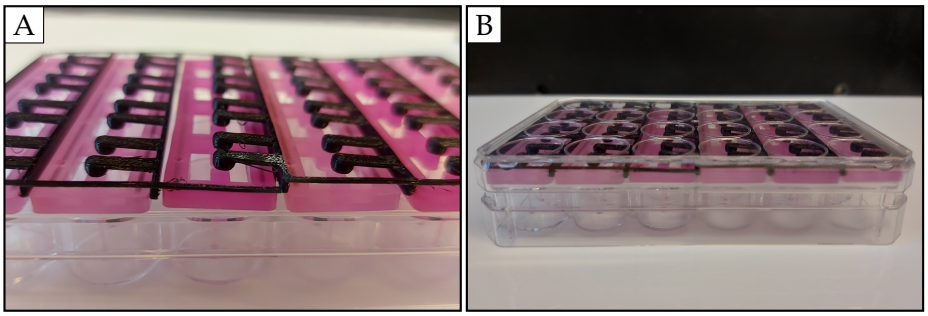


**Figure 1.13:** A) Internal grid placed over the silicon racks; B) Well plate closed containing internal grid and silicon racks.

### SETUP

To apply the force, the device included three main elements described in the table 1.2.

| COMPONENT | DESCRIPTION |
|---|---|
| **Engine** | To generate the required force to stretch the EHTs |
| **Actuator** | To convert the force of the engine in a linear force |
| **External simulator** | To transmit the force from the actuator to the well plate lid |

**Table 1.2:** Main components of the system essentials for the application of the force

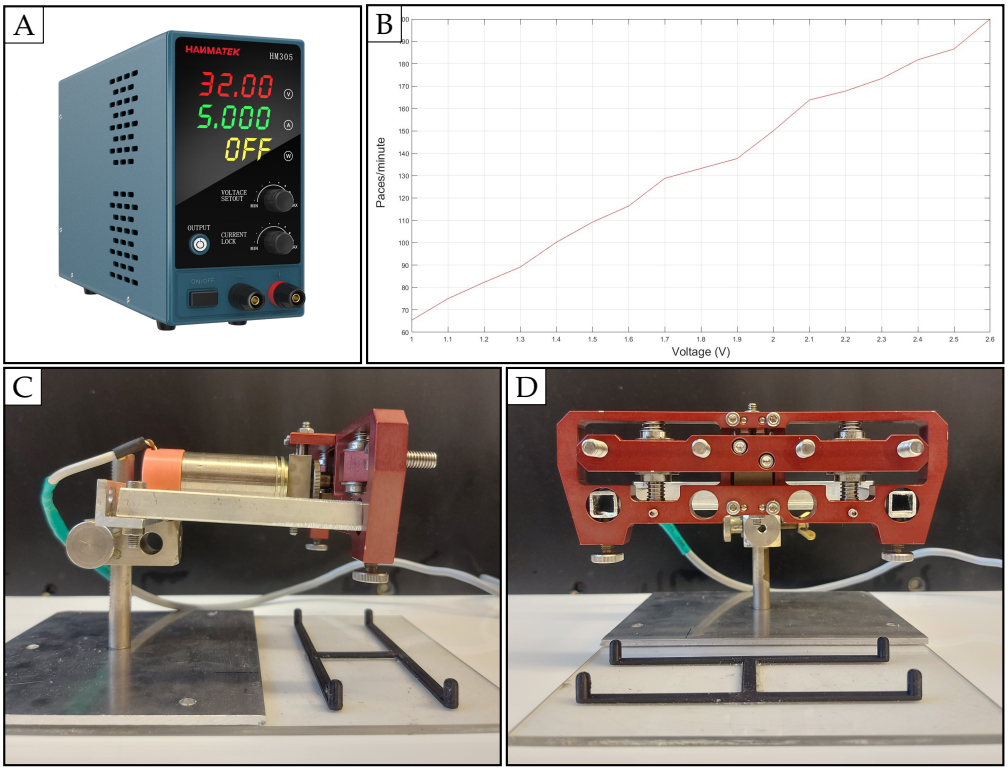


**Figure 1.14:** A) Hanmatek DC Power Supply 30V5A HM305; B) Relation between voltage applied to the engine and paces/minute; C) Side view of the device; D) Frontal view of the device.

**Engine and actuator**

The chosen motor was a direct current (DC) motor and was connected to an actuator (front red part in Figure 1.14C-D) to convert the rotary motion of the motor into linear motion. The engine is powered by a DC power source (Fig. 1.14A). The frequency of mechanical stimulation can be modified by changing the applied voltage. The relation between voltage and paces/minute is reported in Figure 1.14B.
Motor and actuator were supported by a metal structure which is composed of two metal bars that fit into two holes on the actuator. The latter were fixed by two screws that tighten on the metal bars (Fig. 1.14C-D).
The entire structure was glued on a polymethyl methacrylate (PMMA) panel that, thanks to its transparency, allows the observation of the posts deformation from under the structure.

**External stimulator**

The external stimulator was designed to rhythmically apply the desired force to the lid of the well plate (Fig. 1.15B). It consisted of a grid with circular holes, with the same size of the well plate cover, and four supports (Fig. 1.15A). The supports were necessary to fix the external stimulator to the actuator. Performing a cyclic vertical movement, the external stimulator applies a force over the well plate lid and stimulates the EHTs.

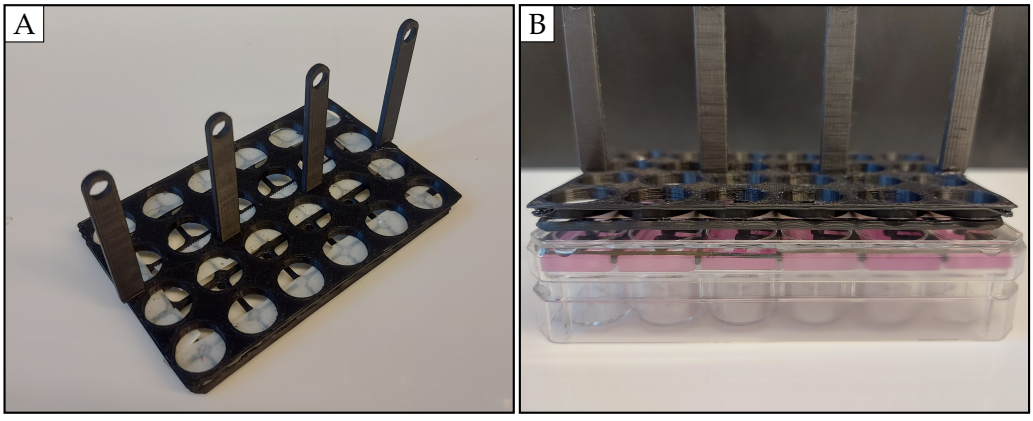


**Figure 1.15:** A) Complete view of the external stimulator; B) External stimulator positioned on the well plate.

A structure that adapts to the well plate was present to keep it in a specific position during the operation of the device (black part H-shaped in Figure 1.14C-D). In Figure 1.16 is reported the complete structure.

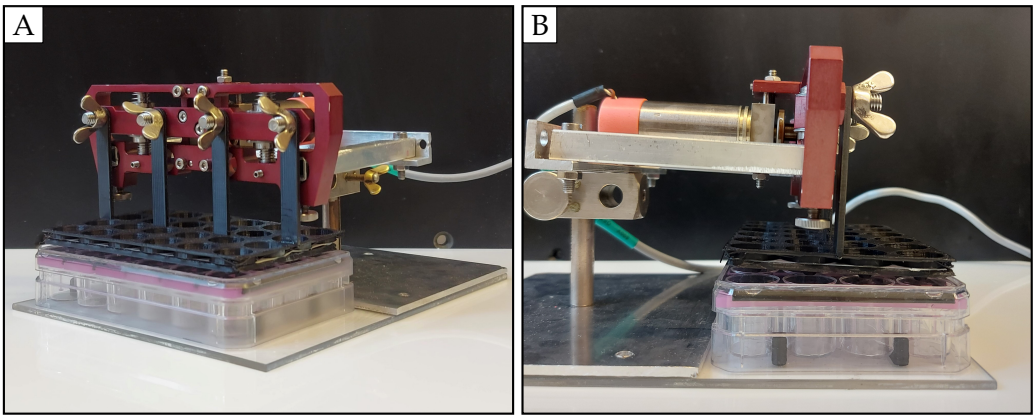


**Figure 1.16:** Complete structure, showing all the external components of the device from the front (A) and from the side (B): actuator (red part), external stimulator (black part), engine (cylindrical part in B).

### 1.4.3 Main problems

The initial configuration of the device presented some problems that led to irregular stimulation of EHTs. The main problems included the instability of the motor and its recoil movements.

**Instability.** As can be observed from the provided images, the whole structure tends to tilt in the direction in which the well plate is positioned (Fig. 1.17A), as the bubble level shows (Fig. 1.17B).
Consequently, the stimulation is non-homogeneous and it depends on the position of each EHT in the plate.

**Recoil movement.** The motor body is not fixed to the PMMA panel. Therefore, at the moment of maximum force application, the engine has a recoil movement resulting in force dissipation.

Additionally, there were two minor issues with the external stimulator and the internal grid.

1. The supports of the external stimulator had a fixed length. As a result, the distance between the actuator and the well plate cover is fixed and the amount of stretching applied to EHTs could not be tuned.

2. The internal grid had a non-symmetric geometry when the symmetry axis was placed between columns 3 and 4 of the well plate (Fig. 1.17C). This resulted in a difference in stimulation between to the right and left of the axis of symmetry.

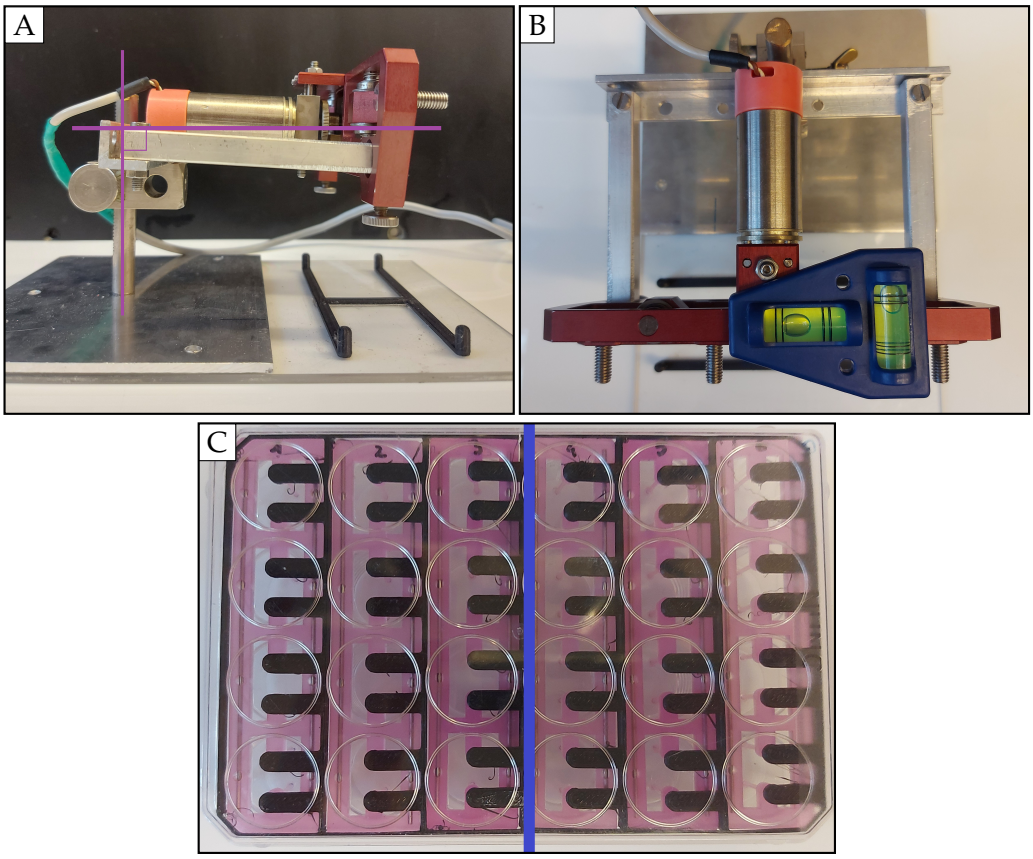


**Figure 1.17:** A) Side view; B) Imbalance of the structure; C) Lack of symmetry in the internal grid.

## 1.5 Aim of the work

The first configuration of the device was unstable and the deformation of the EHTs was uneven. The first aim was therefore to optimize the structural components to make the device more standardized and reduce energy dissipation.
In order to verify the stability of the device before the cell test, it was additionally important to identify a validation method. It was necessary to assess the uniformity and amount of stretching on the racks (without cells) to demonstrate the system's reliability.
The second aim, after optimization and validation, was to test the device on cellular models to provide a preliminary evaluation of the biological effects of mechanical stimulation. These were evaluated by analyzing the force expressed by EHTs and the concentration of specific peptides in the culture media related to cell damage and heart disease conditions.

# 2 Materials and methods

## 2.1 The device

The previous structure was problematic in terms of stability and uniformity of stimulation (Section 1.4.3). Structural components have been designed and produced through 3D printing to solve these problems.

### 2.1.1 3D Printing

3D printing allows to produce components with complex geometries according to computer designs[78]. It is also called Additive Manufacturing (AM) and it involves classes of manufacturing technologies which build 3D components by adding a material layer upon a layer[79]. Seven processes fall into this technique: Stereolitography, Fused Deposition Modeling, Powder bed fusion, Selective laser sintering, Binder jetting, Direct energy deposition, Laminated object manufacturing[80].
These techniques have three basic steps:

1. 3D model design of the component via a dedicated sotware. Fusion 360[81] was used.
2. The slicing of the 3D model to obtain a STL file wich is readable from the 3D printer. IdeaMaker[82] was used.
3. The realization of the component with the chosen printing technique and printer. It was used the Fused Deposition Modeling (FDM) and the 3D printer employed was Raise 3D e2 (Fig. 2.1).

The parts were produced of polylactic acid (PLA), the most widely used in 3D printing.

#### FUSED DEPOSITION MODELING

FDM presents good surface characteristics, it allows the presence of support structure and the processing temperature is low. It can be used with a range of polymers

and it has a low energy consumption. It is advantageous because of the low cost of printing. The printer uses a thermoplastic filament that is heated to reach its melting temperature. This is followed by layer-by-layer extrusion, resulting in the fabrication of a three-dimensional structure[83] (Fig. 2.2).


**Figure 2.1:** Printer model used for component production: Raise 3D e2 printer (https://cianoshapes.com/prodotto/raise3d-e2/).

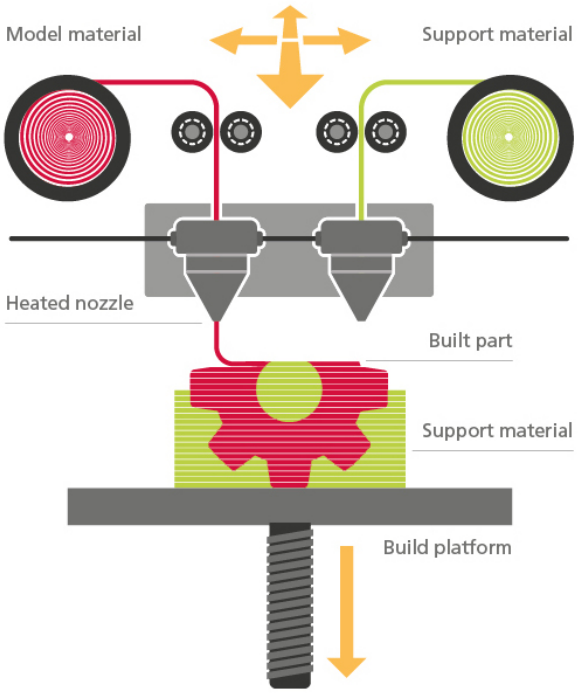


**Figure 2.2:** Components and operation of the FDM technique (https://rapidfab.ricoh-europe.com/technologies/fused-deposition-modelling/).

#### POLYLACTIC ACID

The primary material used in FDM is PLA[84]; all components of the device have been made from this material. It is a bio-plastic that is environmentally friendly and non-toxic to both humans and animals[79].
PLA has been employed in the fabrication of the stimulation grid placed inside the well-plate. Sterilization of this component is necessary to prevent contamination of cell models, since this grid is in contact with silicon racks. Due to the limited crystallinity exhibited by PLA, its heat distortion temperature (HDT) is approximately 55°C. The range of potential applications for PLA is significantly reduced by this restriction[85]. The most used sterilization method in a cellular laboratory is steam autoclave, which reaches up to 121-148°C during the process[86]. For this reason, it is not suitable for sterilizing PLA.
**Sterilization**. The following procedure was used to overcome this issue: after 15 minutes in 70% ethanol, a minimum of 30 minutes of exposure to UV light was performed. A biological safety cabinet was used to carry out all of these steps in a sterile environment.

### 2.1.2 Components

#### ENGINE MOUNT

Motor instability during stimulation was a major problem with the previous configuration. It lacked the ability to fix the engine in a specific position, leaving it free to move during the stimulation and generating recoil movements. This resulted in differences of percentage of stretching across the different wells and energy dissipation.
To prevent this motion and support the motor, an engine holder has been created. It is composed by two parts: a support (Fig. 2.3A) and a locker (Fig. 2.3B) for the engine. The first ensures that the structure is flat, the second avoids recoil movements.
The engine is fixed with the black component positioned above it, through two screws and two wingnuts (Fig. 2.3C). The dimensions of the components are given in Appendix B.1 and B.2.
Precautions have been taken to guarantee that the circular motor body does not rotate and lose its alignment. Two slots are present in the structure to insert two metal bars that fit into the two circular holes on the red structure, guaranteeing a specific location for the stimulation actuator.
A frame of the same dimensions as the 24-well plate has been printed to hold it in

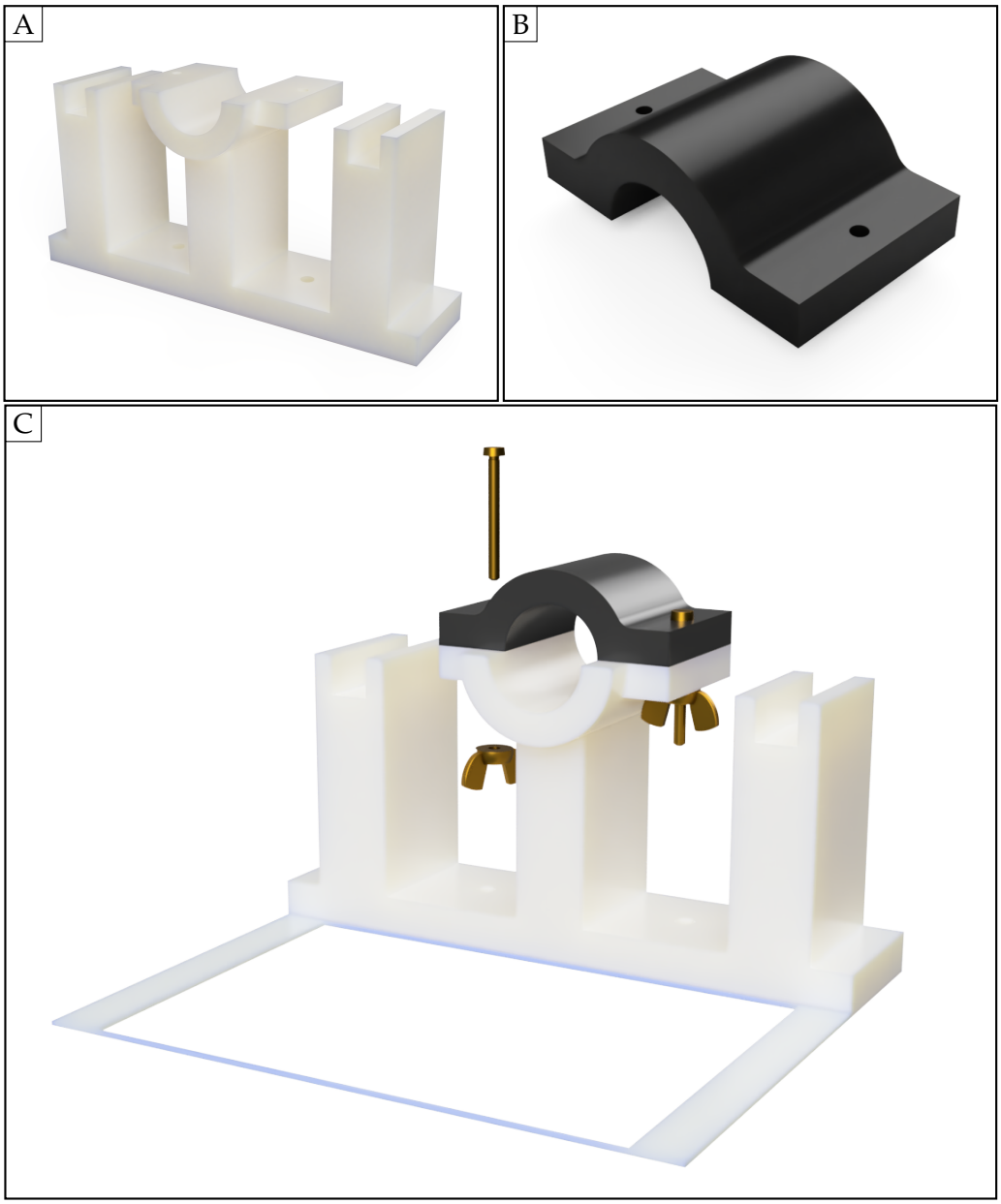


**Figure 2.3:** A) Engine support; B) Engine locker; C) Mounting of the support and the locker.

place during stimulation and to ensure a consistent position every time the 24-well plate is moved (Fig. 2.3C).

### EXTERNAL STIMULATION

To transmit motion from the actuator to the 24-well plate lid, a structure composed of two parts has been fabricated (Fig. 2.4C): a grid with circular holes (Fig. 2.4A) and a support with four rods (Fig. 2.4B). The support is stuck in the grid without the use of glue thanks to two rectangular holes in the grid in which are inserted two protrusions that are part of the support (Fig. 2.4E). Two side hooks prevent relative

rotation movements between the two components (Fig. 2.4D).
The structure has been designed in two parts to obtain a modular component, so the length of the rods can be adjusted to vary the extent of stimulation.
The upper part of the support with the four rods has a larger diameter to prevent material deformation when wingnuts are screwed in.

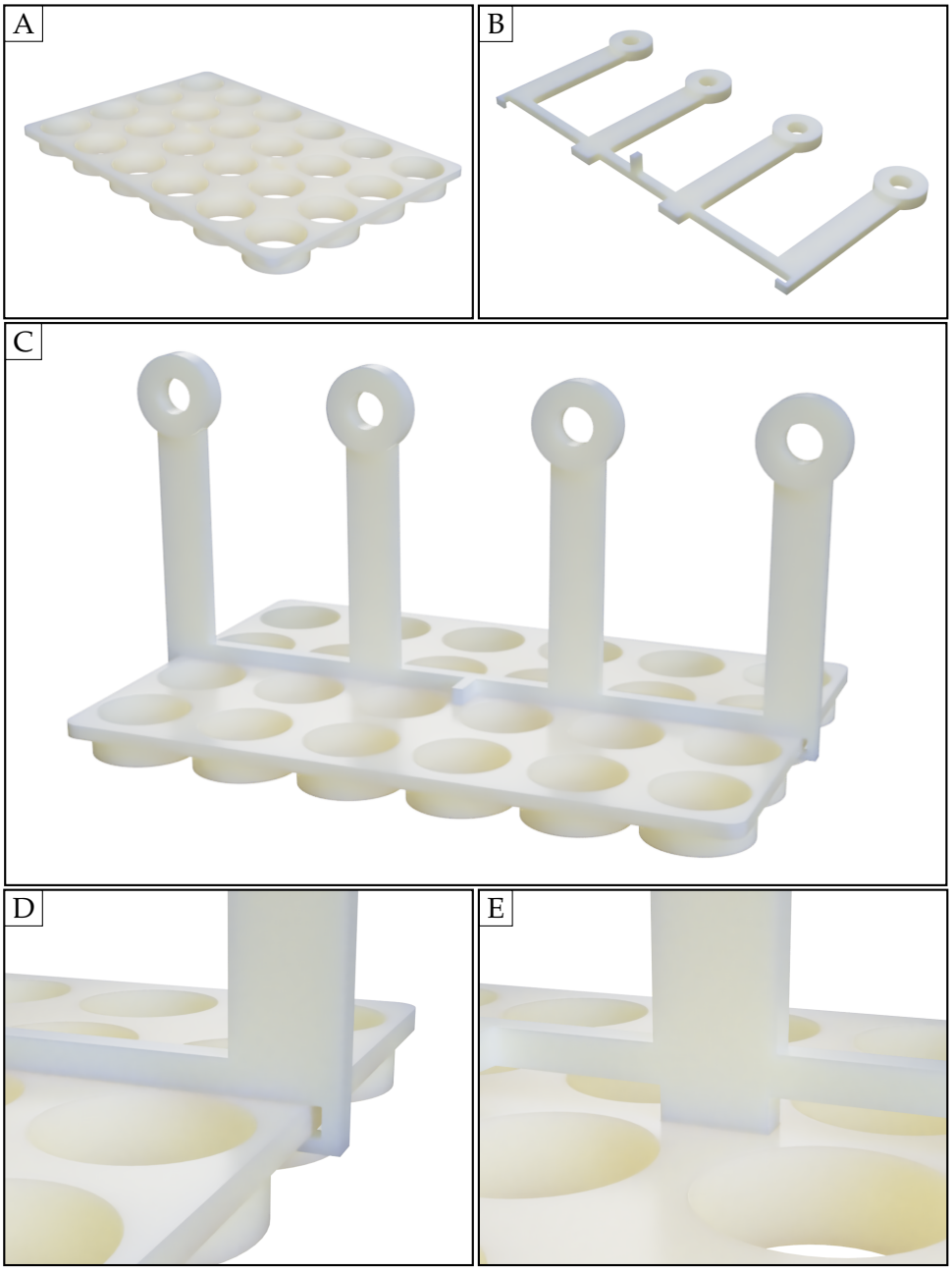


**Figure 2.4:** A) External stimulator grid; B) External stimulator support; C) Complete structure of the external stimulator; D) Lateral hook of the support; E) Joint between the grid and the supports of the external stimulator.

The dimensions of the components are given in Appendix B.3 and B.4.

### INTERNAL GRID

The previous internal grid displayed the issue of asymmetry. As a consequence, during stimulation, a rotational movement of the internal grid structures developed, leading to energy dissipation.
A new grid has been designed to be placed inside the 24-well plate (Fig. 2.5A-B). Two fins have been inserted to improve the positioning. The operating principle remains the same as the previous grid (Fig. 2.5C).
The sterilization method has been proven to be effective, and the geometry ensures that it can be removed and re-positioned easily during medium change operations. All operations must be performed using sterile forceps and under a biological hood. The dimensions of the component are given in Appendix B.5.

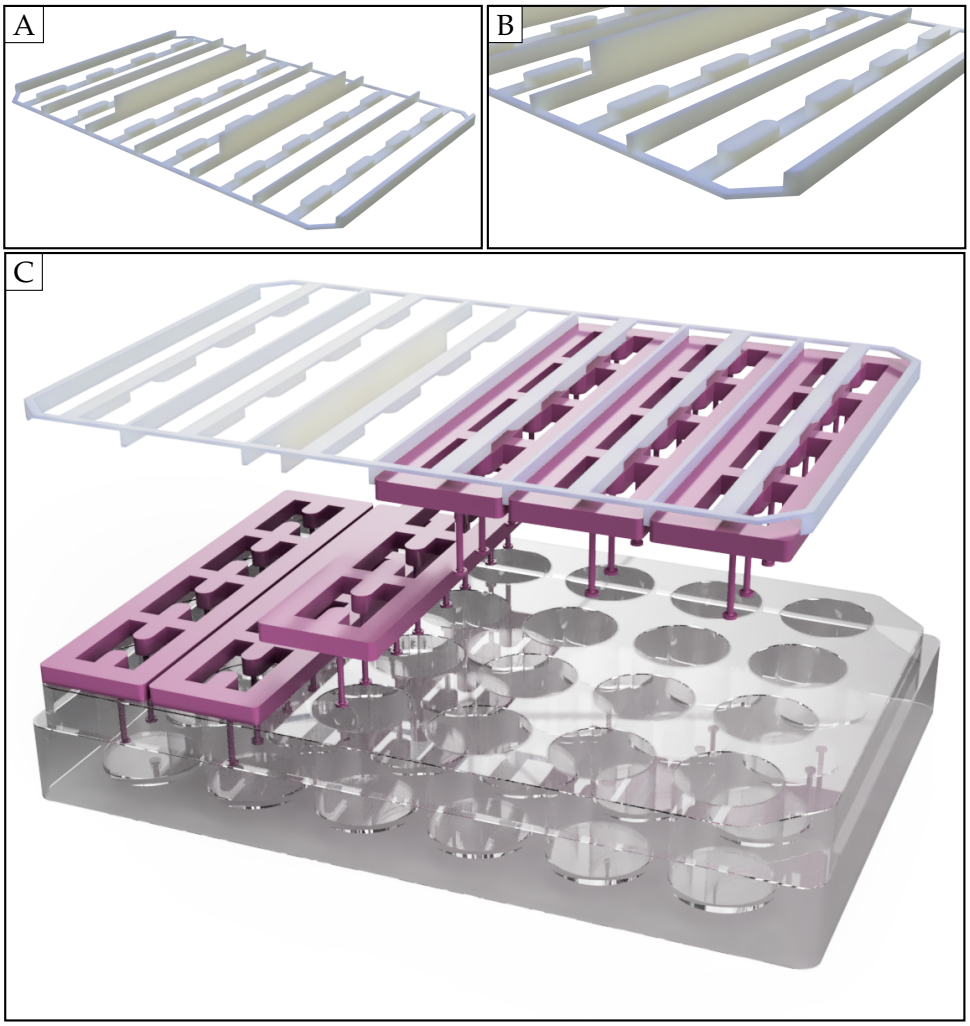


**Figure 2.5:** A) Internal grid geometry; B) Part of inner grid to deform racks.

### ADDITIONAL MATERIALS

The entire structure is assembled using screws. To simplify the installation of the device, wingnuts were chosen to secure each screw within the system. In this way, additional tools are not required to mount the device.
A Multi-Purpose Sealant (DOWSIL™ 732) was employed to glue the motor support and the frame to the PMMA plate, which is both easy to apply and stable from -60°C to +180°C (compatible with incubator environment).

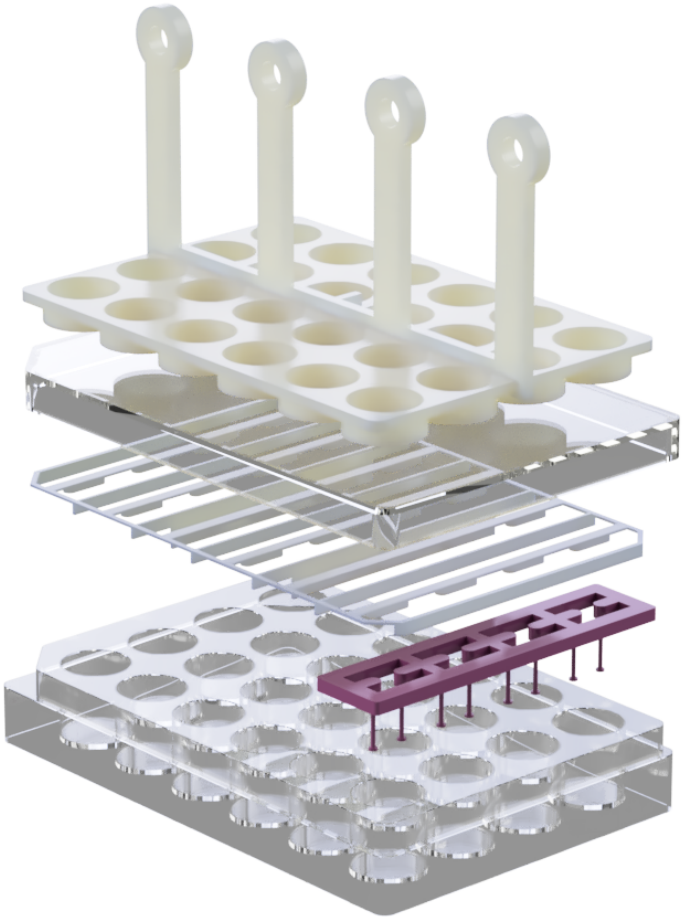

**Figure 2.6:** Illustration of how force is transmitted

### 2.1.3 Device assembling

The engine support and the frame for the well plate must be glued on a panel made of PMMA (Fig. 2.7A). This is important to support the weight of the motor and actuator and to ensure a unique position for well plate. After, the motor is positioned on the support and it is fixed with the locker. Two metal bars prevent its rotation (Fig. 2.7B).

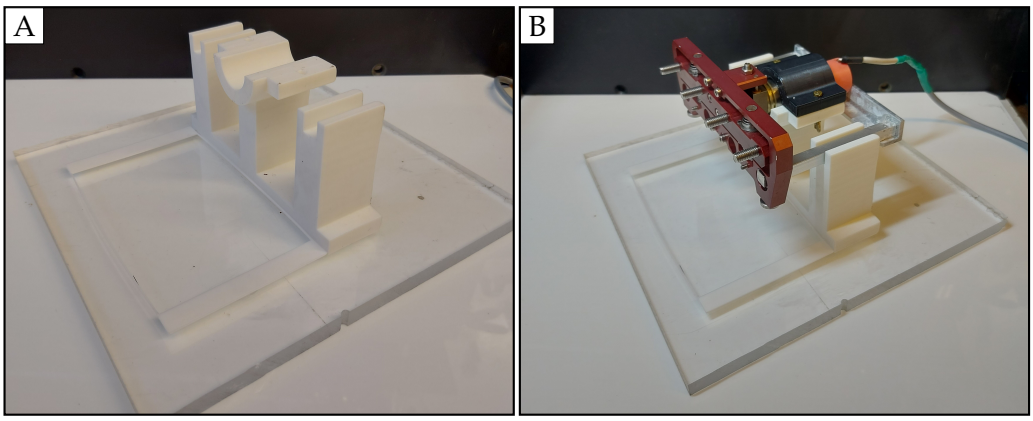


**Figure 2.7:** A) Engine support and well plate frame glued to the PMMA panel; B) Motor fixed to the support.

The external stimulator is assembled by fixing the grid and the support (Fig. 2.8A). The external stimulator is fixed to the actuator through four screws and four butterfly nuts (Fig. 2.8B).

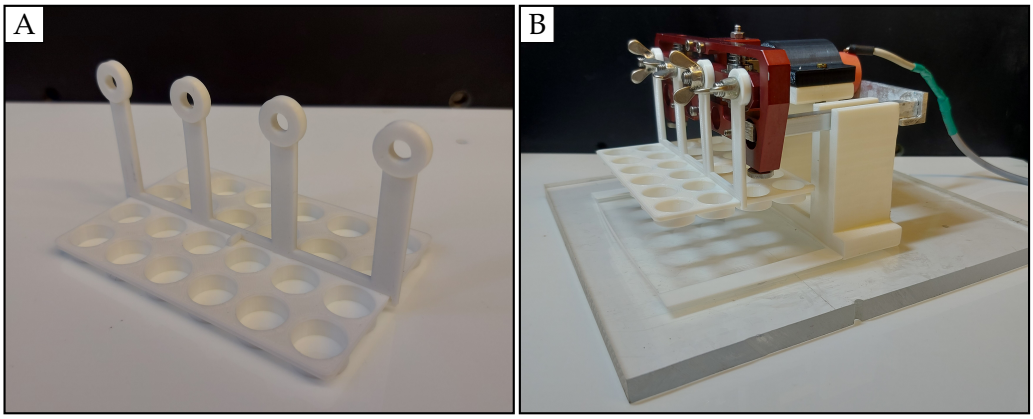


**Figure 2.8:** A) External stimulator assembled; B) External stimulator fixed at the engine holder.

After that the device is sterilized with 70% ethanol and placed in a biological incubator. The connectors are connected to the power source.
The next step is casting heart models, as described in Section 2.2.1. The sterilization of the internal grid is necessary to start the experiment (Section 2.1.1, Polylac-

tic acid, Sterilization). The grid is inserted into the well plate containing the heart models and it is closed with its lid (Fig. 2.9).

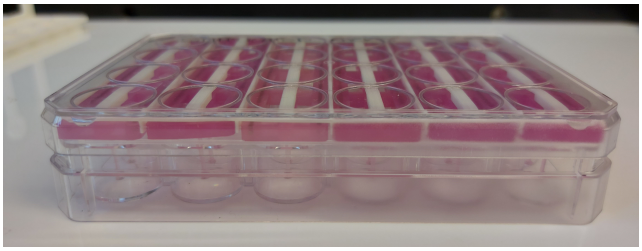

**Figure 2.9:** Positioning of the internal grid

The well plate is placed in the device inside the incubator (Fig. 2.10).
The generator is switched on and the voltage to be applied to the motor is set. This parameter allows to directly choose the frequency of stimulation (Fig. 1.14B).
Stimulation can start by activating the generator.

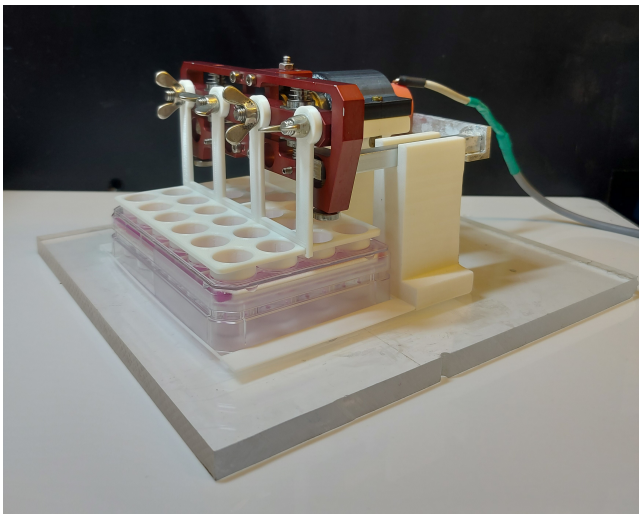

**Figure 2.10:** Complete setup

The heart models chosen need the change of the media on Monday, Wednesday and Friday. During this operation it is important to use a sterilized forceps to move the internal grid to maintain the sterility.

### 2.1.4 Stretching measurement

#### CAMERA

To evaluate the stretching of the posts, 10-second videos were recorded and subsequently analyzed. A standard computer webcam, Logilink UA0072, was used. A mount has been printed (Fig. 2.11A) to ensure that the camera is positioned at the

same distance from the samples every time videos are recorded (Fig. 2.11B). The dimensions of the component are given in Appendix B.6.

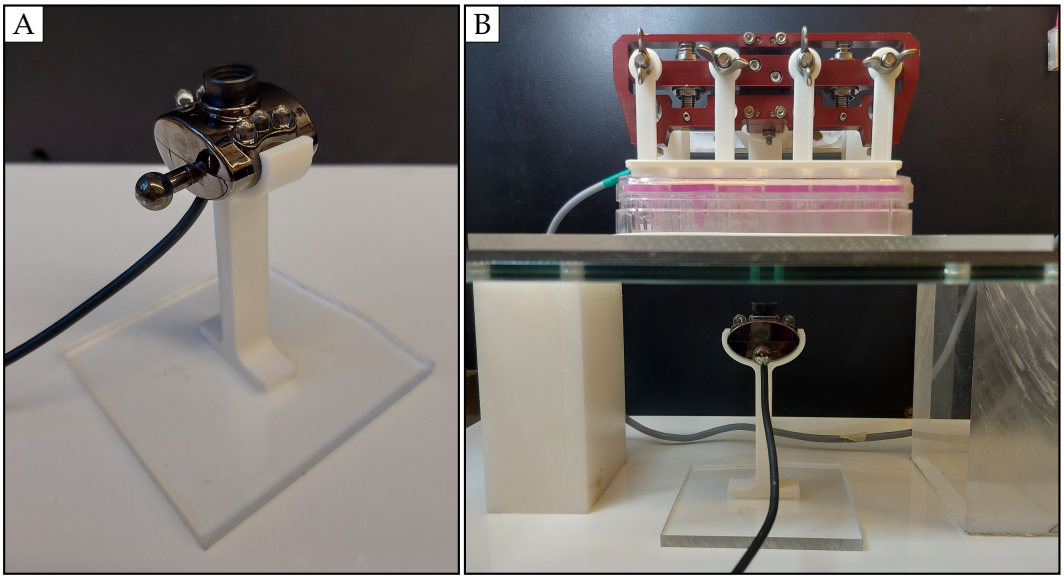


**Figure 2.11:** A) Camera holder; B) Positioning during the recording of videos.

### MATLAB CODE

The objective of the optimization was to achieve uniform stimulation across the entire well plate platform. The uniformity of stimulation was evaluated using a measurement tool. For this purpose, a MATLAB[87] code was developed using the Computer Vision Toolbox plugin. The analysis involves recording 10-second videos, capturing the wells from below using the described camera. Subsequently, the videos are analyzed using MATLAB, which tracks the movement of the posts, selected by the user at the beginning of each video (Fig. 2.12A), and measures the distance between the posts in pixels for all frames. The analysis ends with the calculation of the percentage displacement of each pair of posts in relation to the non-stimulated position. Through a dialog window the analysis is shown in real time for each video (Fig. 2.12B).

At the end of the analysis, the code generates and saves three different graphics: a heat map of all wells values, a bar graph of mean values on the well plate rows (A, B, C, D) and a bar graph of mean values on the well plate columns (1, 2, 3, 4, 5, 6) (Fig. 2.12C-D-E). The uniformity of stimulation can be evaluated by comparing the values of all wells. The presence of stimulation patterns can be possibly identified from the bar charts.

The MATLAB code has been validated using videos of varying lengths and it is reported in Appendix A.

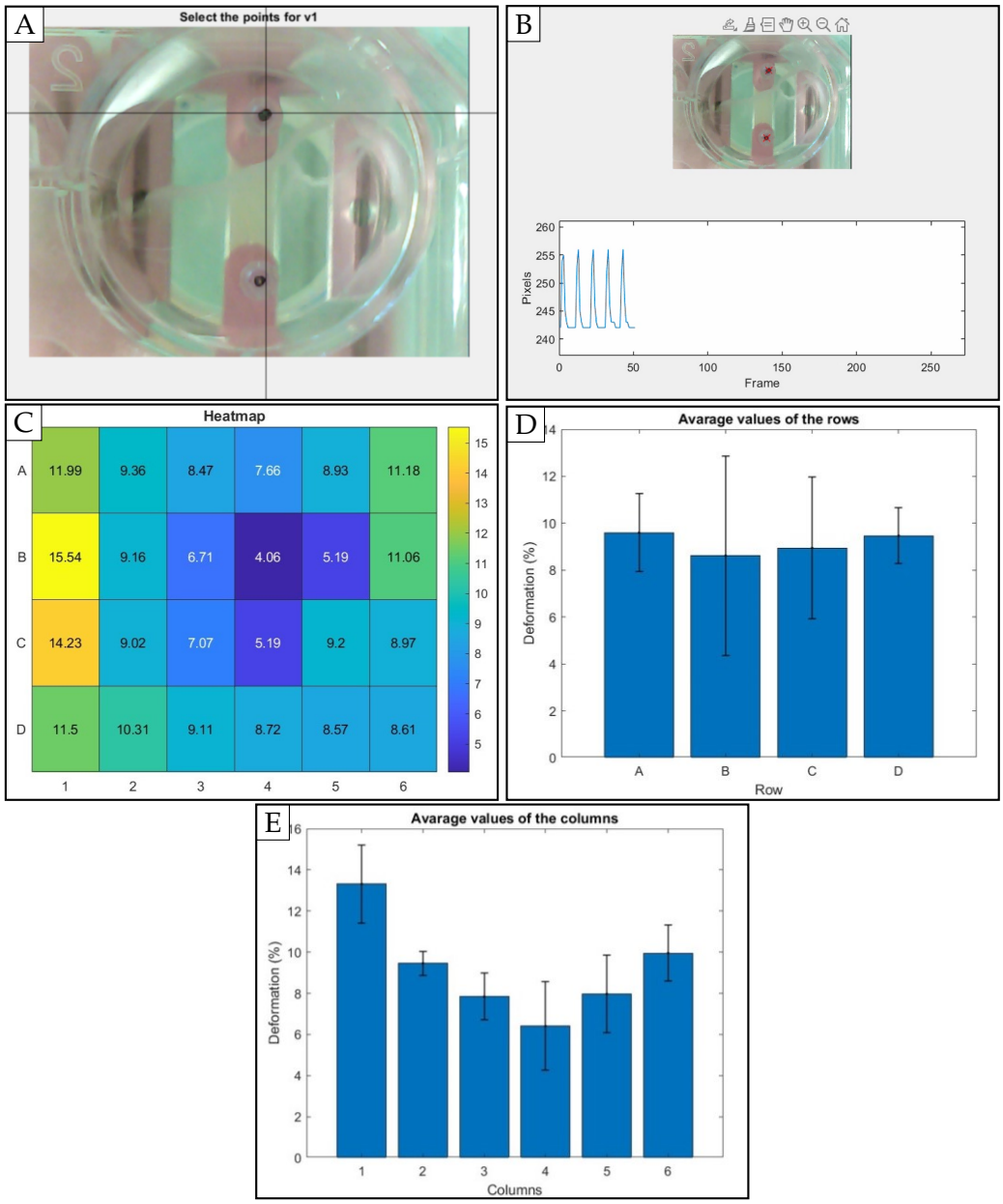


**Figure 2.12:** A) Real-time view of the analysis; B) Dialog window to select points of interest; C) Heat-map of all wells values; D) Average values on the well plate rows; E) Average values on the well plate column. Error bars display SD.

## 2.2 EHTs

### 2.2.1 Casting

The method for casting fibrin-based engineered heart tissue (EHT) in standard 24-well culture dishes is described below[88]. This protocol requires standard equipment for cell culture, including all reagents and instruments, except for spacers and silicon racks.

Materials:

- Aprotinin
- Fibrinogen
- Thrombin
- Agrose 2%
- 10× Dulbecco's modified Eagle medium (DMEM)
- 2× DMEM
- EHT medium
- ERC001 hiPSC cell line (1 mln/EHT)
- Cell culture microplates, 24-well
- Spacer (Fig. 2.13A)
- Silicon racks (Fig. 2.13B)

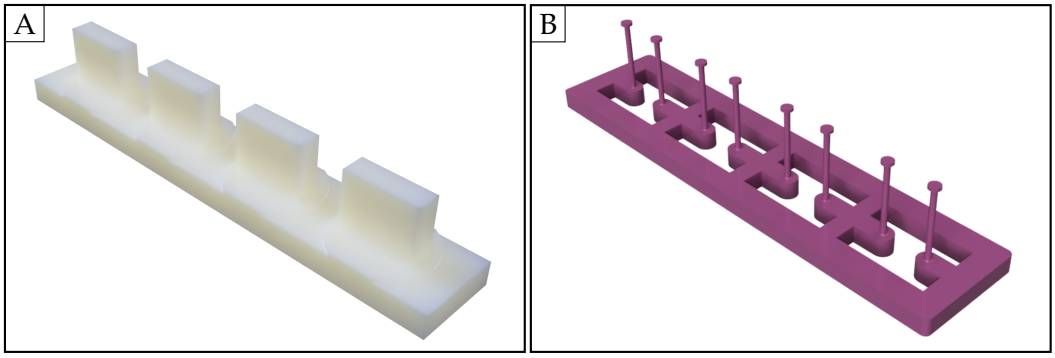


**Figure 2.13:** A) Spacer to obtain the mold for the EHTs; B) Racks used as support for the EHTs.

Protocol (Fig. 2.14):

a) Place 1.6 ml of agarose solution in each well of a 24-well cell culture plate by pipetting. Each well column requires a PTFE spacer, totaling 6 spacers on a 24-well plate.

b) Solidification will take 15 minutes to complete. During solidification prepare the master mix with the desired cell number.

c) Remove spacers and place silicon racks, one for each column

d) Mix 97 µl of mastermix with 3 µl of thrombin and pipet the mixture immediately into the agarose mold. Place the well plate in a cell incubator (37 °C, 7% $CO_2$, 40% $O_2$) for 80 minutes. Pipet a small amount of medium for each well and incubate for at least 10 minutes.

e) Prepare a well plate containing 1.5 ml of EHT medium for each well and transfer the silicon racks with the EHTs.

f) After approximately two weeks, the CMs have established a network throughout the body, beating in unison and producing force.

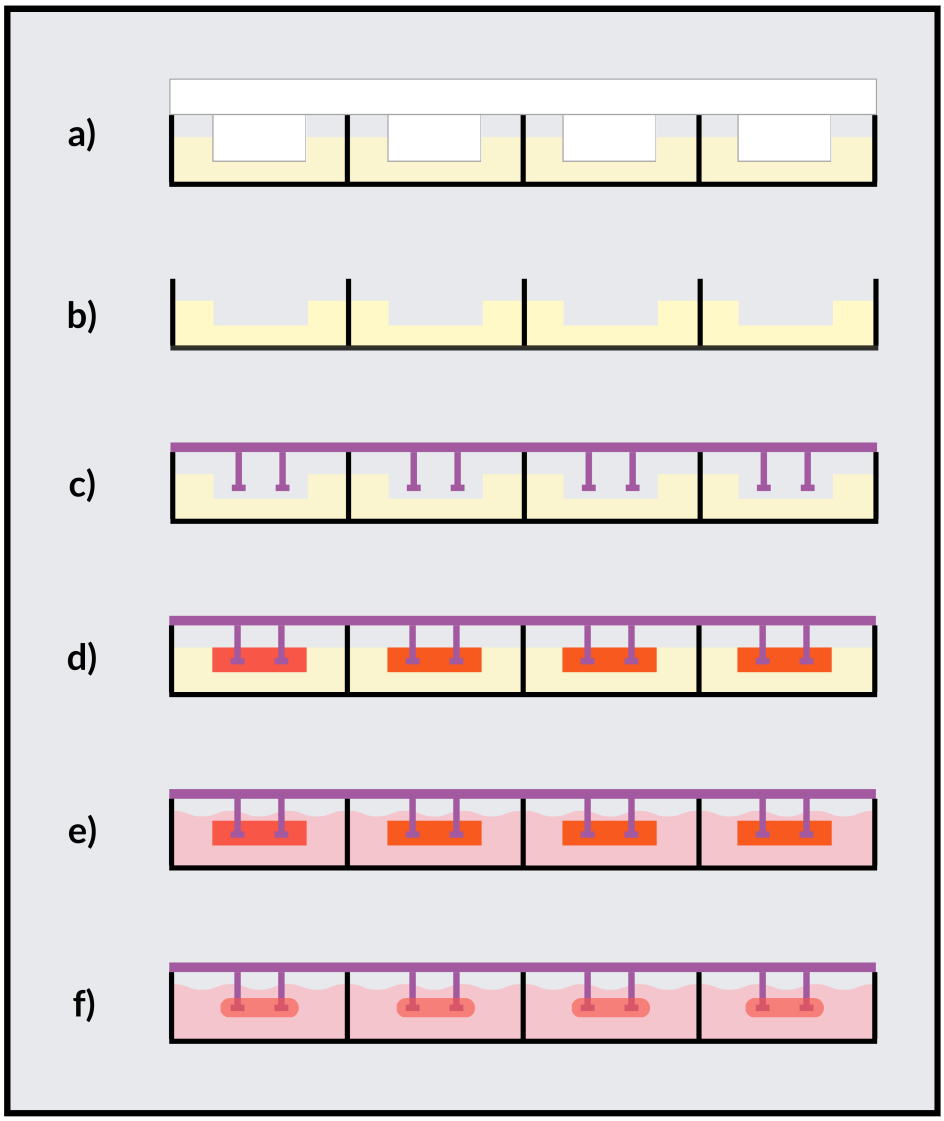


**Figure 2.14:** Steps for casting the EHTs.

### 2.2.2 Stimulation

A total of 48 EHTs were cast and divided into two 24-well plate, with the purpose of obtaining 24 stimulated models and 24 control models.
The EHTs were cultured for 25 days. On the 25th day, the models were considered mature (as described in Section 2.2.1), and the stretching of the 24 EHTs (a complete 24-well plate) started.
Stimulation was carried out continuously for a period of 7 consecutive days, at a stimulation frequency of 2.5 Hz, on the 24 selected models. The remaining 24 control models were kept under standard culture conditions. A higher frequency of stimulation than physiological was chosen to induce a pathological condition.
During this period, the culture medium was changed on Monday, Wednesday and Friday, with a brief interruption of stimulation of approximately 20 minutes for each medium change.

### 2.2.3 Analysis

#### CONTRACTION ANALYSIS

The impact of stimulation was evaluated through video-based optical analysis (Fig. 2.15), developed in the laboratories of the Institute of Experimental Pharmacology and Toxicology at University Medical Center Hamburg-Eppendorf.

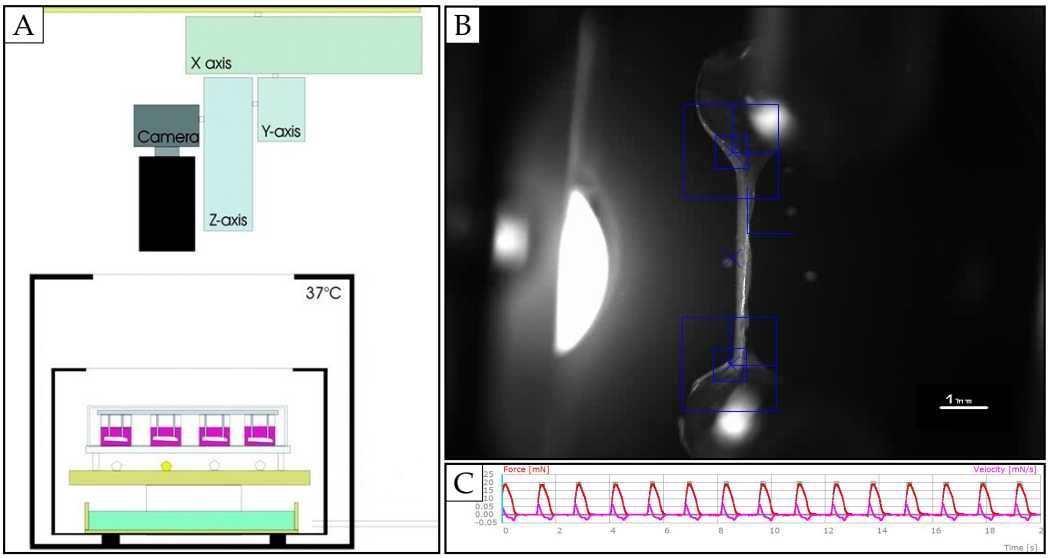


**Figure 2.15:** A) Video Optical analysis system; B) Live image of the model; C) Graph shows contractions over time (adapted from xy).

The system comprises a cell incubator equipped with controls for regulating $CO_2$ levels, humidity, and temperature (Fig. 2.15A). In order to visualize the models,

light-emitting diodes were positioned under the well plate. The activation of the lighting system and the video recording process are synchronized to minimize the elevation of the culture medium's temperature. The videos (Fig. 2.15B) are captured using a Basler camera (Type A 602f-2). The camera's position in the XYZ direction is managed by a computer running custom software (CTMV, Pforzheim, Germany). This software is capable of recognizing figures and, consequently, identifying contractions, beating frequency, average force, fractional shortening, and contraction-and-relaxation times[85] (Fig. 2.15C). All models were analyzed with this technique at every medium change.

**MEDIUM ANALYSIS**

To assess the cellular response to stimulation, after 7 days of stretching, the culture medium was analyzed to measure the concentrations of N-terminal pro B-type natriuretic peptide (NT-proBNP) and Troponin I (TnI), related to heart stress, volume-related issues and myocardial damage. The medium was collected separately for each model.

**N-terminal pro B-type natriuretic peptide.** NT-proBNP is the N-terminal fragment of the B-type natriuretic peptide (BNP). BNP is mainly synthesized and secreted by myocytes in the left ventricle (LV) as a response to myocytes stretched by pressure overload or volume expansion of the ventricle[89]. It is located on chromosome 1 and encodes the 108 acid pro-horomne proBNP[90]. Upon release into the circulation it is cleaved in equal proportions into the biologically active 32 amino acid residues (AAR) BNP, which represents the C-terminal fragment, and the biologically inactive 76 amino acid N-terminal fragment (NT-proBNP)[91] (Fig. 2.16).
The use of NT-proBNP as a marker of cardiac function and as a risk factor for atrial fibrillation can help detect heart failure[92]. It is preferred to use NT-proBNP as a marker because it has a half-life six times longer than BNP, which is why the serum concentration is higher for NT-proBNP than for BNP[91].
The evaluation of the concentration of NT-proBNP is important to verify the effective mechanical stretching of EHTs; it was performed with the ARCHITECT BNP assay.

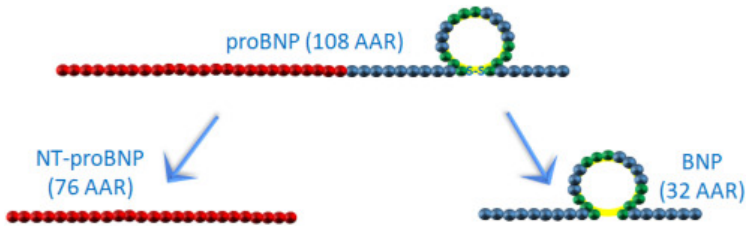


**Figure 2.16:** Pathways of NT-proBNP and BNP synthesis from proBNP[93].

**Cardiac Troponin I.** Cardiac Troponin I (cTnI) is a protein in the CMs that regulates the Calcium-mediated interaction between actin and myosin[94]. It is part of a complex of three different subunits: Troponins I (cTnI), C (cTnC) and T (cTnT) (Fig. 2.17A). The $Ca^{2+}$ regulation of the contractile interaction takes place in the presence of all three subunits of Troponin and of tropomyosin[95]. cTnT and cTnI are suitable for the detection of myocardial damage because they are released into the bloodstream as a result of heart muscle cells death[96] (Fig. 2.17B). However, due to its increased specificity and sensitivity, TnI is the preferred choice for detecting acute myocardial infarction, also because its cardiac isoform exhibits greater dissimilarity to TnI from other tissues[96].
This protein was chosen to verify that the mechanical stimulation did not damage the cells causing cell death.

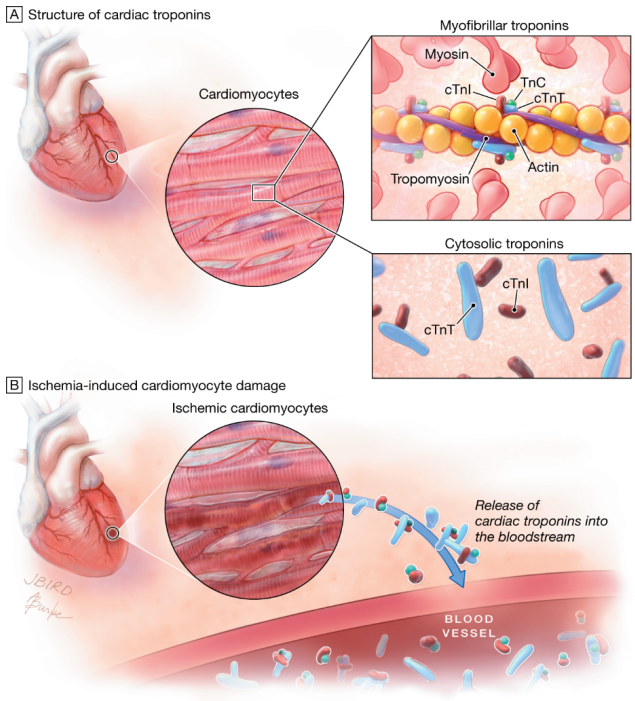


**Figure 2.17:** Mechanism of release of cardiac troponin after ischemic cardiac injury[97].

### 2.2.4 Statistical analysis

For the statistical analysis of the data, GraphPad Prism 8 software was employed, recognized for its reliability and versatility in biomedical statistics. The analyses utilized the Two-Way Analysis of Variance (ANOVA) method. To identify significant differences among groups, Tukey's multiple comparison tests were conducted, considering a significance threshold with a p-value set at 0.05.

# 3 Results and discussion

## 3.1 Optimization

The optimization of the device was achieved thanks to the use of FDM printing technology and PLA material. The instability problems were solved by the design of new structural components. The result was a flat structure, as shown by the spirit level (Fig. 3.1B), and the absence of recoil movements.

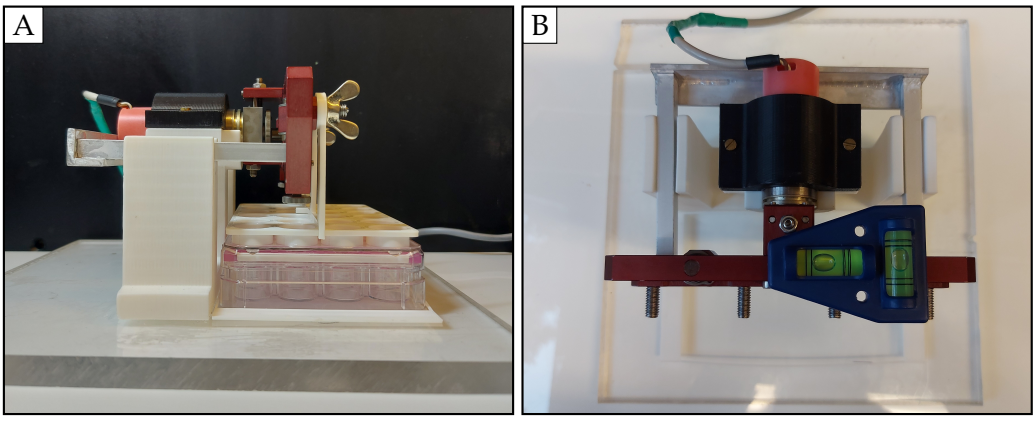


**Figure 3.1:** A) Lateral view of the device demonstrating the achieved stability; B) Test with the spirit level to verify that the device is level.

The device was simple to produce and to assemble; no additional tools were needed to mount it. The internal grid was easy to handle and, following the instructions defined in this work, no cases of bacterial or fungal contamination had occurred.

## 3.2 Stretching validation

Matlab software was used to analyze the percentage of rack deformation before performing cell testing. This code allowed for the selection of two points of interest and provides real-time visualization of post movement and the variation in distance between the two posts (measured in pixels). Two tests were performed to validate the system.

**Frequency variation**

The reaction of the components of the instrument to variation of the stimulation frequency was analysed. One set of six racks was tested at three different stretching frequencies which were chosen to be in the range of the spontaneous beating frequency of atrial EHT (2 Hz, 2.4 Hz, 2.8 Hz). The analyses indicate that the behavior of the device remained consistent as the stimulation frequency increased (Fig. 3.2A-B), but it resulted in reduced deformation (Fig. 3.2C).

**Different racks**

The reproducibility of the stimulation properties of the system was additionally tested on eighteen racks divided in three groups (SET1, SET2, SET3), stimulated all at the same frequency. Variability in percentage of stretching could be observed, however mainly attributed to the racks used for casting the EHTs. These racks are not single-use and they are sterilized after each use. During this process, they may undergo deformations that affect the way the racks are stretched. This was confirmed by analyzing the deformation of racks in different sets. A varying degree of non-uniformity was observed based on the specific racks used (Fig. 3.3A-B). Therefore, this suggests that variability of stretch was not due to an inherent device imbalance, as the pattern did not repeat consistently with different racks, but rather an influence of rack non-uniformity.

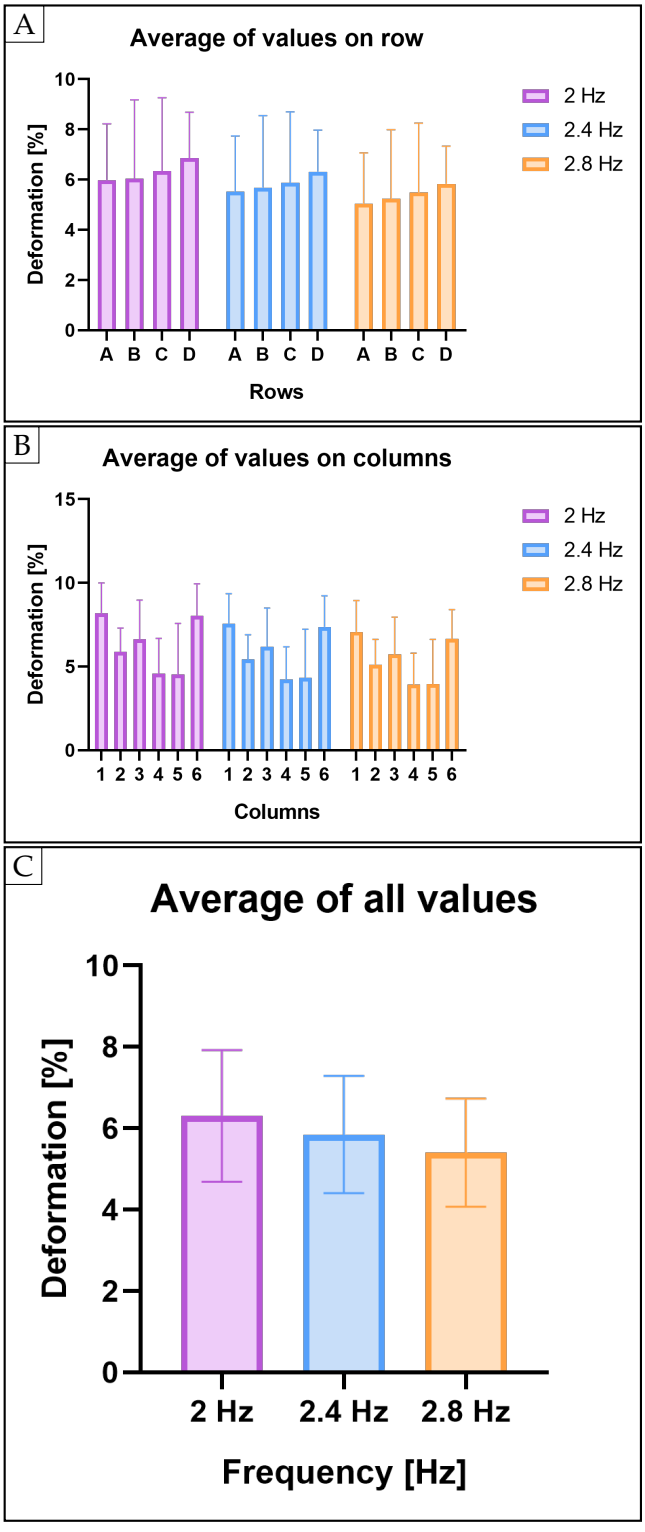


**Figure 3.2:** A) Average of values on rows at different frequencies; B) Average of values on columns at different frequencies; C) Average values for the entire well plate at different frequencies. Error bars display SD.

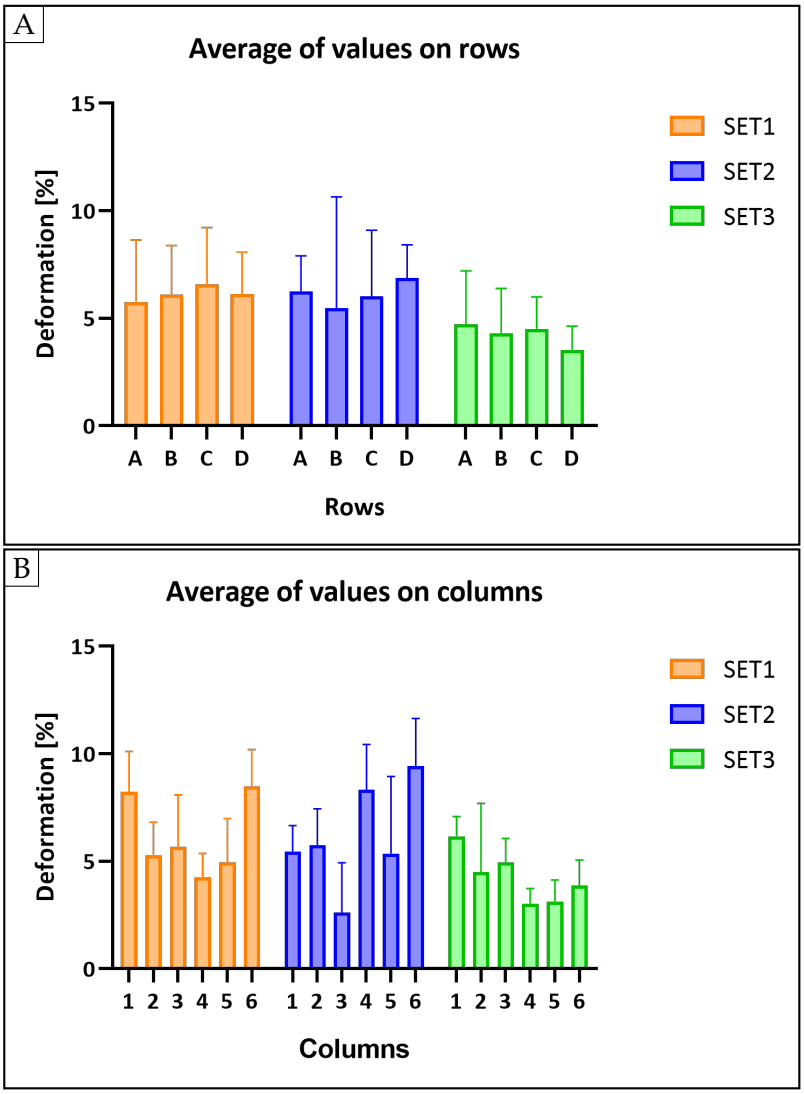


**Figure 3.3:** A) Average of values on the rows with different set of racks; B) Average of values on the columns with different set of racks. Error bars display SD.

## 3.3 EHTs

24 EHTs were stretched for 7 days after 25 days of maturation. At the end of the experiment, the racks used for EHTs casting were analyzed with the Matlab system, without EHTs, to assess the intrinsic variability of the racks. This analysis enabled the determination of the percentage of stretching that each EHT had undergone. Six EHTs were selected for the analysis: three highly stimulated and three medium stimulated. The values of force and the concentration of bio-marker peptides released by the EHTs placed in these wells were collected and compared with the respective properties of un-stretched controls (three control samples were selected).

### 3.3.1 Force evaluation

The evaluation of the force expressed by EHTs was performed with the so called White-box system. Contractility was measured at every medium change. Each group included three samples ($n = 3$), described before. The average value of the force was calculated for each group and compared with the control group (Fig. 3.4A-B) using GrpahPad 8.0 software. Day 0 refers to the situation before the stimulation, after 25 days of maturation; day 7 is the last day of stretching. The average value of each group was normalized with the force value on day zero. In this way the variation of the force across the stimulation period in percentage was quantified.

The graphs show a decrease of the force developed by stretched EHTs. From the data collected, this reduction was higher for medium stimulated samples rather than for highly stimulated samples, as could have been expected (Fig. 3.4A). A significant difference was observed on the last day of stretching, between control and medium stretched samples (Fig. 3.4B).

These results contrast with previous studies of mechanical stretching of heart tissue in which researchers observed an increase in the force expressed by the samples following stimulation[98,99]. However, the aim previous research was to utilize subtle stretch as physiological load to promote cardiac tissue maturation and spontaneous contraction of CMs. In this project however, the observation of the effects of mechanical stretching on mature tissues was the objective, to replicate pathological conditions of variable and pathologically increased preload *in vitro*. Ovchinnikova et al.[76] performed a similar experiment, highlighting a lower force expressed by the stretched samples compared to the control group, that are in line with those obtained in this project. The decrease of the expressed force was observable from

the video recorded by the White-box system.

### 3.3.2 Medium analysis

It was important to assess the presence of factors of cellular damage and cellular stretching. On the final day of stretching, the culture media of the sample of interest was analysed and NT-proBNP and cTnI concentrations were determined. The graphs represent the average value for each group (Fig. 3.4C-D)

**NT-proBNP.** It is known as a higher level of NT-proBNP released from cardiac tissue indicates a cardiac stretching[100]. The data analysis about the NT-proBNP concentration in the culture media on the last day of stimulation show a trend towards a higher concentration, indicating a greater release for the stretched samples (Fig. 3.4C). Consistent with force data, medium stretched samples produced more NT-proBNP than highly stretched ones.

**cTnI.** cTnI is a indicator for damage to CMs and it is released e.g. in case of myocardial infarction. In accordance with this study, several other provided *in vitro* evidence that mechanical stretching increases the release of cTnI from CMs[101–103]. Again, cTnI concentration was higher in the media of medium stimulated samples rather than that of of highly stimulated samples (Fig. 3.4D).

Both NT-proBNP and cTnI values showed no significant difference. This is probably due to the fact that few samples were analysed.

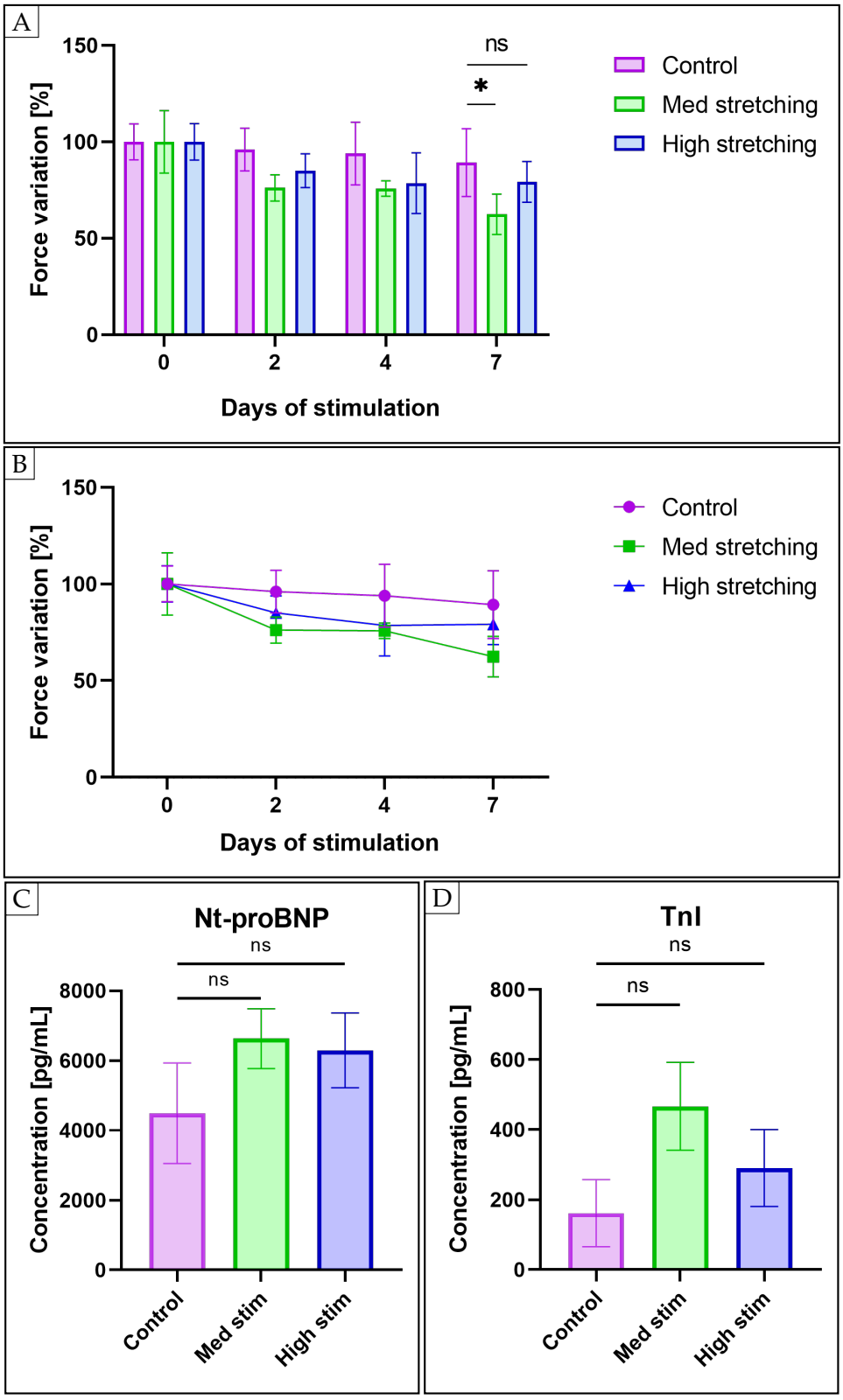


**Figure 3.4:** A) Force evolution over time for each sample group; B) Comparison of developed by EHTs from each group for each time point; C) Media NT-proBNP concentration on the last day of stimulation; D) Media cTnI concentration on the last day of stimulation. Error bars display SD.

# 4 Conclusions and future perspectives

The thesis work aimed to obtain a standardized way to develop a *in vitro* model of pathological heart tissue. To achieve this objective, a device to apply cyclic mechanical stretching on EHTs was developed and optimized. The mechanical stimulation applied on EHTs by the system induced mechanical stress with the physical stretching of CMs, providing an *in vitro* representation of volume overload, e.g. in heart failure. Moreover, it can be used to mimic heart rate abnormalities (e.g. arrhythmia, tachycardia, bradycardia) by varying the stimulation frequency applied on EHTs. The device was optimized but it is a prototype and still presents some instabilities. After another optimization phase, it could become a useful tool to better investigate cardiac pathological mechanisms and to have a heart *in vitro* model to test new drugs and therapies in the preclinical stage.

## 4.1 The device

The optimization of the device was achieved through the fabrication of new structural components to support the motor during the system activity, support and locking for the motor, and new parts for the application of force on cardiac models, internal grid and external stimulator. This was possible employing FDM technology, a fast prototyping and manufacturing method, using PLA as process material. The motor support and locking ensure a flat position for the cylindrical motor and prevent recoil movements during stimulation. In addition, maintaining the engine in a define position during the experiment reduces the energy dissipation. The flat position ensure a homogeneous stimulation of all EHTs, because the external stimulator is parallel to the well plate cover and it applies the pressure evenly everywhere.

Thanks to the design of the 3D printed components, it was able to mount and as-

semble the device without using any additional tools, giving the possibility for an user friendly mounting procedure, independently from the placing of the well plate containing the EHTs. This allowed the lowering of contamination risk, since the sterile parts are not in contact with the stimulation system. The only printed part involved in the stimulation mechanism in contact with EHTs, is the grid. However, it was demonstrated that this part is easy to sterilize as it has a simple geometry and can be sterilized with simple procedures. Following the protocols described in this work, no bacteria or fungi contamination was spotted during test.

The amount of stretching applied on EHTs can be adjust and modulated by different parameters as the voltage and the external stimulator height. This component, in fact, is modular, since the four rods can be designed with different length, providing a different stretching intensity. The stimulation frequency can be easily tuned by varying the voltage applied to the engine, as shown in Figure 1.14B.

Matlab was employed to develop a code able to analyse video. During the analysis, the silicon posts are followed to calculate the percentage of stretching performed by the device. This percentage is calculated in relation to the un-stretched position of the posts. Using the Matlab code, the percentage of stretching for each pair of posts can be measured, allowing the analysis of the uniformity of stimulation. At the and of the analysis three graphs showing the data are saved: an heat-map with all the values, a bar chart with the average values for the columns and a bar chart with the average values for the rows.
Since during Matlab analysis variability of the stretching between different wells was observed, two tests were performed to understand the reasons of the instability. The first was the evaluation of the effects of the variation of the voltage applied to the engine to vary the stimulation frequency. The second was the measuring of the percentage of stretching using different racks (18 racks divided in 3 groups) to evaluate their influence on the uniformity of stimulation. The results showed that system was consistent at different frequencies, but there was a decrease in the percentage of stretching applied to the posts with the increase of the frequency. This behaviour was the same for the whole well plate. Using different racks, it was observed that the difference in the percentage of stretching between the wells were given by the racks themselves. The reason was that the racks are not disposable and after the use they are sterilized. During this process the silicon racks are subjected to a deformation of both the frame and the posts. For this reason, they were not all in the same geometrical condition during the experiment. e.g. some of them were tilted.

After that, a set of new racks (never undergo sterilization process to remove rack deformation variable) was analyzed with Matlab (Fig. 4.1A). It was observed a pattern of stimulation and the samples placed in the center of the well plate were less stimulated than samples on the edge. This was caused by the well plate lid which is convex and had more resistance in the middle. To overcome the problems of the well plate lid and the inevitable deformation of the racks for the sterilization process, the solution could be to produce a new well plate lid with the 3D printing technique, including the internal grid (Fig. 4.1C-D). In this way the original well plate lid is substitute with a more resistant cover, which does not bend during stimulation. In addition, a grid would be used to fix the silicon racks in a specific position, reducing the effects of deformed rack (Fig. 4.1B).

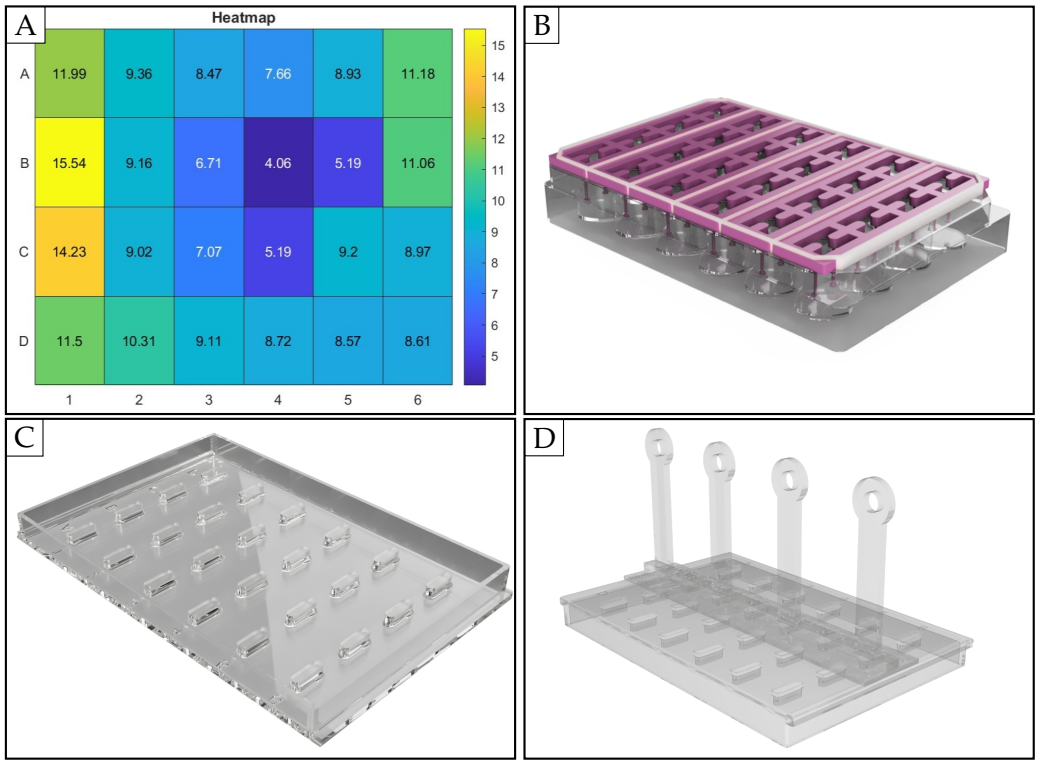


**Figure 4.1:** A) Heat-map with the percentage of stretching related to a set of new racks (never undergo sterilization process to remove rack deformation variable); B) Gird to fix the deformed racks in a defined position during the stimulation; C) Proposal of a new lid for the 24-well plate that allows to integrate the external stimulator with the internal grid; D) Complete structure of the new external-internal stimulator.

## 4.2 Cellular test

The chosen heart *in vitro* model was the mini-EHT developed by Hansen et al[77]. It is a fibrin-based hydrogel casted around two flexible silicon posts, with embedded CMs. Thanks to presence of the two silicon posts, the cells develop autonomously contractile activity after about 10 days. They need around 25 day to be considered mature. The contractility was analyzed with a video-based optical system, able to quantify beating frequency, average force, fractional shortening and contraction-and-relaxation times.

After the device optimization, cellular test was conducted. Two 24-well plate with EHTs were casted to have one plate as control and one stretched plate. The stimulation started after 25 days from the casting, time necessary for the complete maturation of the EHTs, and it was performed for 7 days.

It was decide to quantify the variation of force over time to evaluate the effects of the mechanical stretching over the EHTs. Before starting the stimulation, force expressed by EHTs was measured. It was measured during all the experiment for both stretched and un-stretched samples at every media change day (Monday Wednesday, Friday). At the end of the experiment, data from stretched samples were collected and compared with the control samples. Analyzing the racks used for the casting of the stimulated models, six EHT were selected: three medium stimulated and three highly stimulated. Three random sample from the control plate were chosen. It was detected an high standard deviation calculating the mean value of force for each group analyzed, attributed to the intrinsic variability of EHTs. For that reason, to compare the variation of force between the groups, the average value of the force at every time points was normalized with the value before the start of the stimulation for each group. The comparison of the trend of the force over time between control, medium stretched and highly stretched samples showed a more marked reduction in force for those stretched, in particular for the medium stretched EHTs. Trough statistical analysis, a significant difference was observed between the control and the medium stretched EHTs on the last day of stimulation.

Two peptides were selected, TnI and NT-proBNP, to evaluate the cell viability after seven days of stimulation and to assess how much EHTs felt the stimulation. TnI and NT-proBNP concentration on the EHTs media the last day of stimulation was quantified. Again, it was collected only the media of the samples of interests for each group (control, medium stretched, highly stretched). TnI concentration was

higher for stretched samples, in particular for those medium stretched. As reported by different studies, this is a standard behaviour for CMs subjected to mechanical stress. This result was consistent with the results obtained from force analysis.
NT-proBNP concentration was evaluated because it is a biomarker secreted by CMs in the left ventricle (LV) as a response to CMs stretched by pressure overload or volume expansion. It is also a marker used in clinic to detect the risk of atrial fibrillation and hart failure. It is now consolidated that an higher level of NT-proBNP released from CMs indicates a cardiac stretching. From the comparison between the groups, a trend towards a higher concentration for the stretched samples. As for the previous analysis, the effects were more evident for the medium stretched EHTs.

## 4.3 Final consideration

At the end of the project it was possible to state that the system was optimized: it is consistent and stable at different frequencies. During the cellular test, a response from the EHTs was observed, through a decrease of contractility and a higher production of stretching marker (TnI and NT-proBNP) for the stimulated samples. This indicated a trend towards a pathological condition of the cardiac tissue.
There are still some limitations because the effects of the racks deformation on the stimulation is still present and the data about the peptides concentration did not show a significant difference, so other experiment should be conducted.
Finally, also if the device has still some instability, it is a promising way to develop a standardizes method to induce pathological conditions in heart tissue, eventually in combination with other physical stimuli (e.g. electrical, optogenetic).

# Appendices

# A Matlab code

```
clc
clear all

% Select the folder
folder = uigetdir();
if folder == 0
    error('No folder seleceted.');
end

dateTime = datestr(now, 'yyyy_mm_dd_HHMM');
name = [dateTime,'_Results'];

% Final results folder
pathRes = fullfile(folder,name);
if ~exist(pathRes, 'dir')
    mkdir(pathRes); %creation of the folder
end

% Find all the mp4 files
files = dir(fullfile(folder, '*.mp4'));
numFile = numel(files); %numero di file con questa
   estensione

% Results
res = cell(numFile, 4); % Well, Min distance, Max distance,
   FS

%% ANALYSIS OF EVERY VIDEO
for i = 1:numFile
```

```
% Upload of the video
video = VideoReader(fullfile(folder, files(i).name));

% KLT Tracker
tracker = vision.PointTracker('MaxBidirectionalError',
    1);

% Read the first frame
frame = readFrame(video);

% Select the points
imshow(frame);
title(['Select the points for ',video.name(1:end-4)]);
punti_iniziali = ginput(2); % select 2 points

% Tracker with starting point
initialize(tracker, punti_iniziali, frame);

close

dist = [];

% Video analysis
while hasFrame(video)

    % Read the current frame
    frame = readFrame(video);

    % Track the points
    [pointTrak, isTracked] = tracker(frame);

    % Calculate the distance between the points
    if sum(isTracked) == 2

        distFrame = norm(pointTrak(1, :) - pointTrak(2,
            :));
```

```
            % Add the distance to the array
            dist = round([dist, distFrame]);

        end

        % Show the points real time
        subplot(2,1,1)
        imshow(frame);
        hold on;
        plot(pointTrak(:, 1), pointTrak(:, 2), 'rx', '
           MarkerSize', 8);
        title(files(i).name(1:end-4));

        % Show the distances real time
        subplot(2,1,2)
        plot(dist);
        xlabel('Frame');
        ylabel('Pixels');
        xMin = 0; xMax = video.NumFrames;
        yMin = min(dist)-5; yMax = max(dist) + 5;
        axis([xMin xMax yMin yMax]);

        hold off; drawnow;

    end

    close;

    % Percentage calculation
    av = mean(dist);
    distNorm = dist - av;

    [peak_pos, loc_pos] = findpeaks(distNorm, 'MinPeakHeight
       ', 0);

    neg_distanze = -distNorm;
    [peak_neg, loc_neg] = findpeaks(neg_distanze, '
       MinPeakHeight', 0);
```

```
peak_pos = peak_pos + av;
peak_neg = -peak_neg + av;

av_pos = mean(peak_pos);
av_neg = mean(peak_neg);

FS(i) = round((av_pos-av_neg)/av_neg*100,2);

% Show the results
f = figure(2);

plot(dist); hold on
plot(loc_pos, peak_pos, 'g*'); hold on
plot(loc_neg, peak_neg, 'r*'); hold on

xMin = 0; xMax = video.NumFrames;
yMin = min(dist)-5; yMax = max(dist) + 5;
axis([xMin xMax yMin yMax]);

yPos = zeros(video.NumFrames,1); yNeg = zeros(video.
   NumFrames,1);
xPos = 1:video.NumFrames; yPos(:) = av_pos;
xNeg = 1:video.NumFrames; yNeg(:) = av_neg;

plot(xPos,yPos,'g'); hold on
plot(xNeg,yNeg,'r'); hold on

title('Results');
xlabel('Frame');
ylabel('Pixels');

pause;
close

% Add the resutlts to the table
res{i, 1} = files(i).name(1:end-4);
res{i, 2} = av_neg;
```

```
    res{i, 3} = av_pos;
    res{i, 4} = FS(i);

    % Release il tracker
    release(tracker);
end

%% SAVE THE RESULTS

% Table with the final results
tabRes = cell2table(res, 'VariableNames', {'Well', 'Dist_min
   ','Dist_max', 'Percentage'});

% Save the results in excel
nameExcel = fullfile(pathRes, [dateTime,'_Data.xlsx']);
writetable(tabRes, nameExcel, 'Sheet', 'Dati', '
   WriteRowNames', true);

%% GRAPHs
dataFin = NaN([6,4]);
numElem = min(numel(tabRes.Percentage),numel(dataFin));

dataFin(1:numElem) = tabRes.Percentage(1:numElem);

dataFin = dataFin';

% Heatmap
name = [dateTime,'_Heatmap.jpeg'];
xvalues = {'1', '2', '3', '4', '5', '6'};
yvalues = {'A','B','C','D'};

figure; % Heatmap with all values
c = colormap('default');
h = heatmap(xvalues,yvalues,dataFin,"Colormap",c,'Title',['
   Heatmap ',dateTime]);

saveas(h,fullfile(pathRes,name)); % save the figure
```

```
clear xvalues yvalues h name

% Bar charts
nameRow = 'Bar_chart_row.jpeg';
nameCol = 'Bar_chart_col.jpeg';

xRow = categorical({'A','B','C','D'});
xRow = reordercats(xRow,{'A','B','C','D'});
xCol = categorical({'1', '2', '3', '4', '5', '6'});
xCol = reordercats(xCol,{'1', '2', '3', '4', '5', '6'});

yRow = mean(dataFin,2); dsRow = std(yRow);
yCol = mean(dataFin); dsCol = std(yCol);

figure; % Bar chart for rows
chartRow = bar(xRow,yRow); hold on
errorbar(xRow, yRow, dsRow, 'black', 'linewidth', 1);
title(['Rows ',dateTime]); xlabel('Row'); ylabel('
   Deformation (%)');

saveas(chartRow,fullfile(pathRes,nameRow)); % save the
   figure

figure; % Bar chart for columns
chartCol = bar(xCol,yCol); hold on
errorbar(xCol, yCol, dsCol, 'black', 'linewidth', 1);
title(['Columns ',dateTime]); xlabel('Columns'); ylabel('
   Deformation (%)');

saveas(chartCol,fullfile(pathRes,nameCol)); % save the
   figure

close all

fprintf('Analysis completed.');
```

# B Drawings of the components

## B.1 Engine support

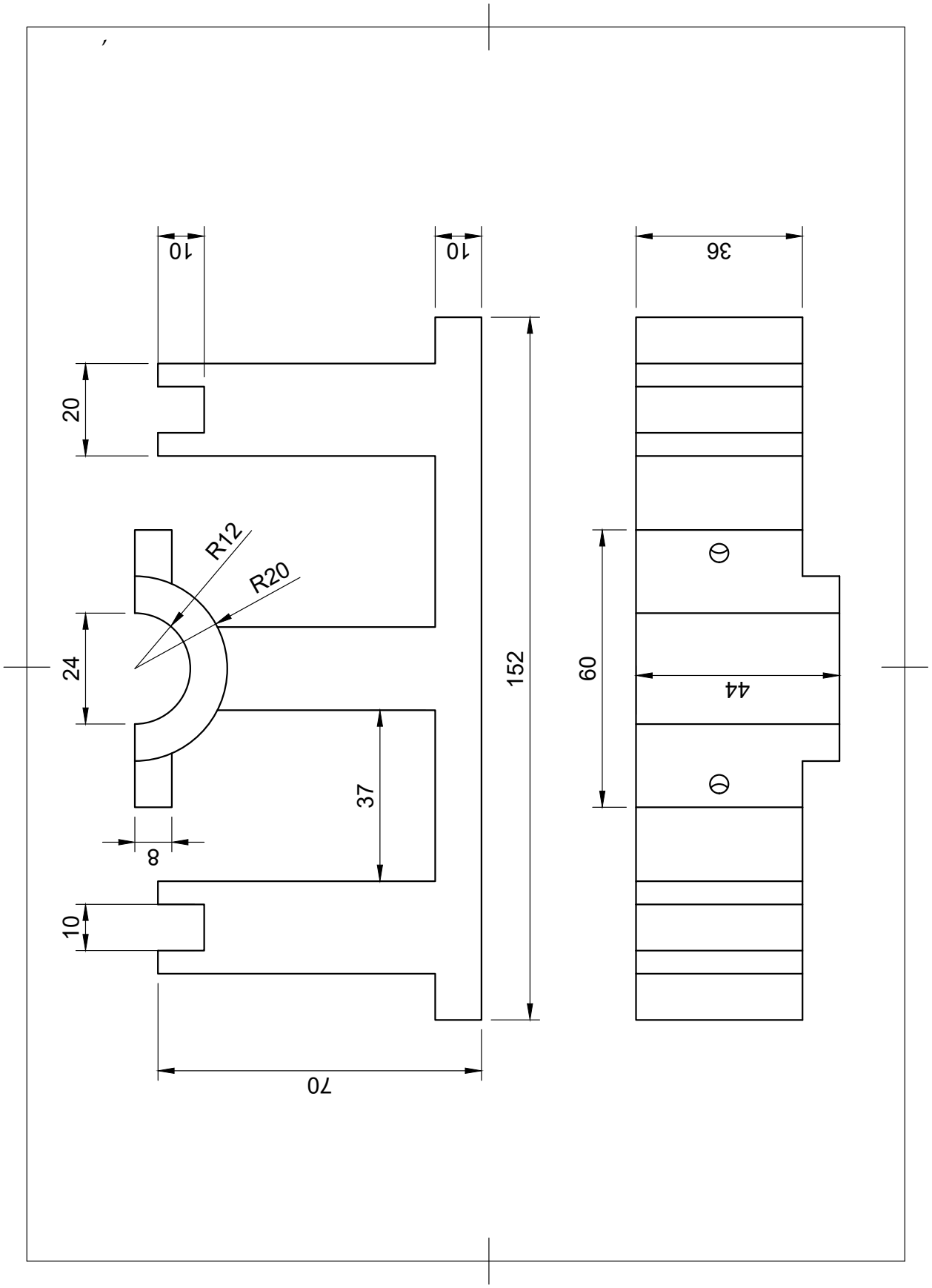

## B.2 Engine locker

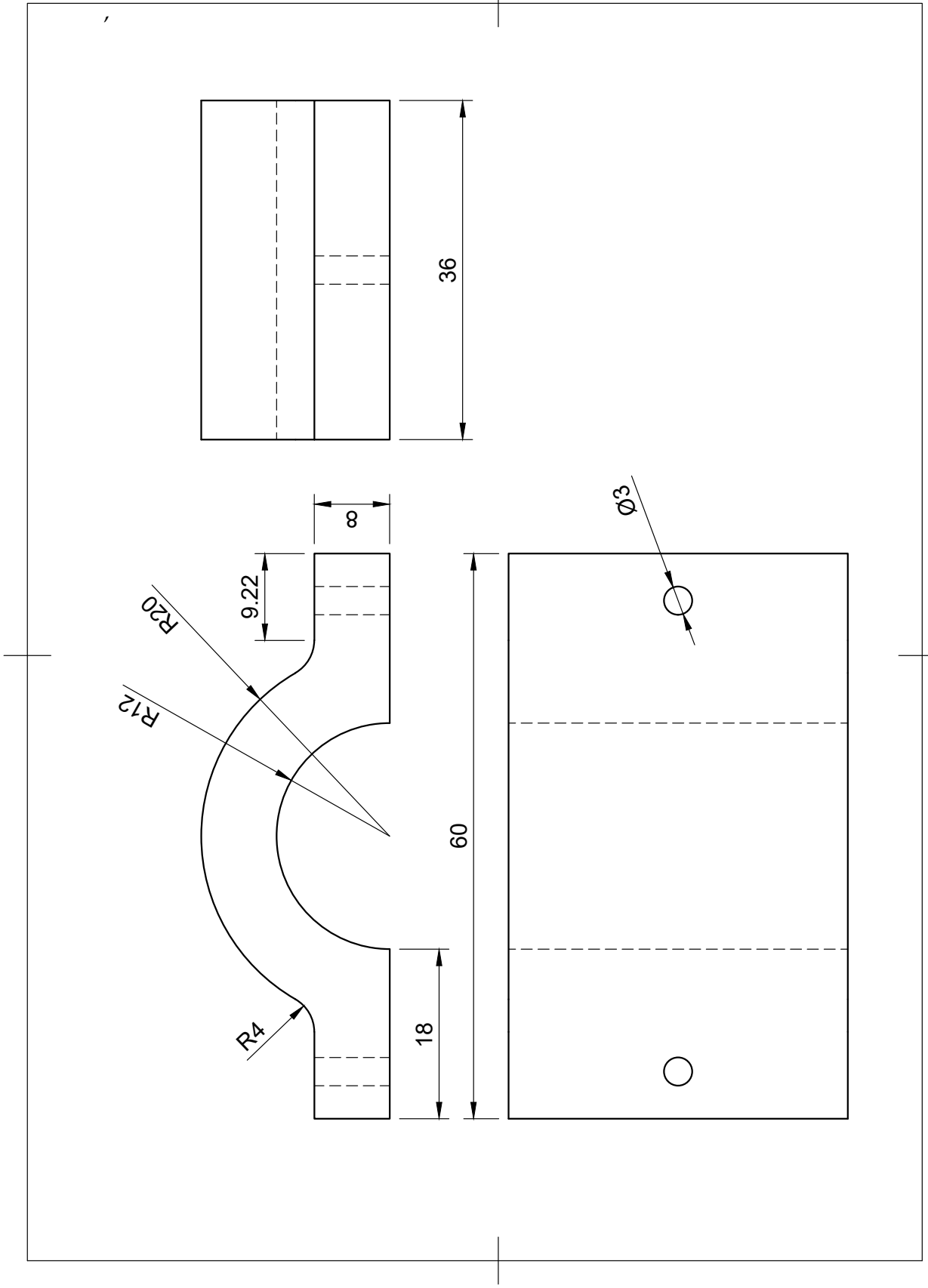

## B.3 External stimulator grid

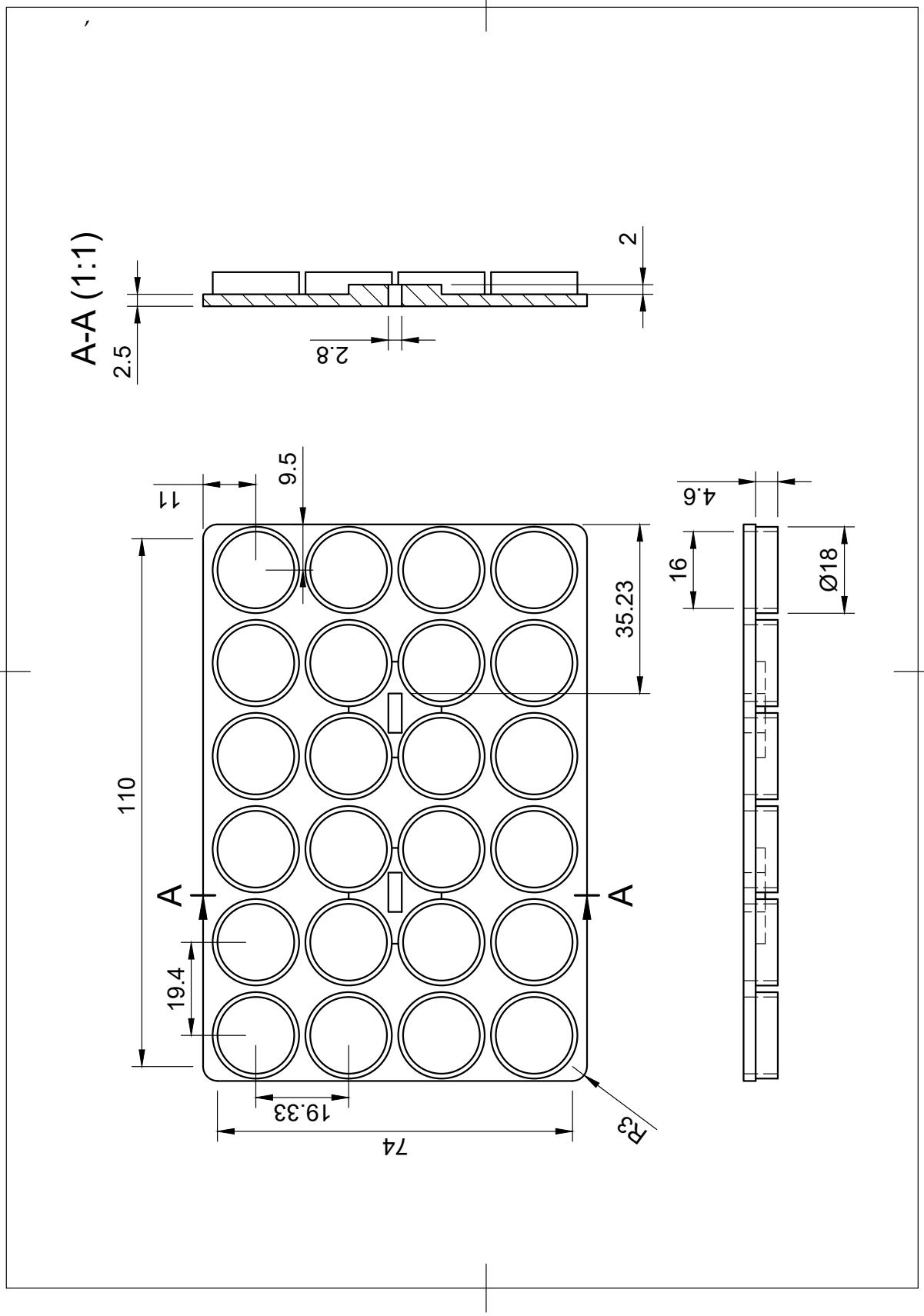

## B.4 External stimulator support

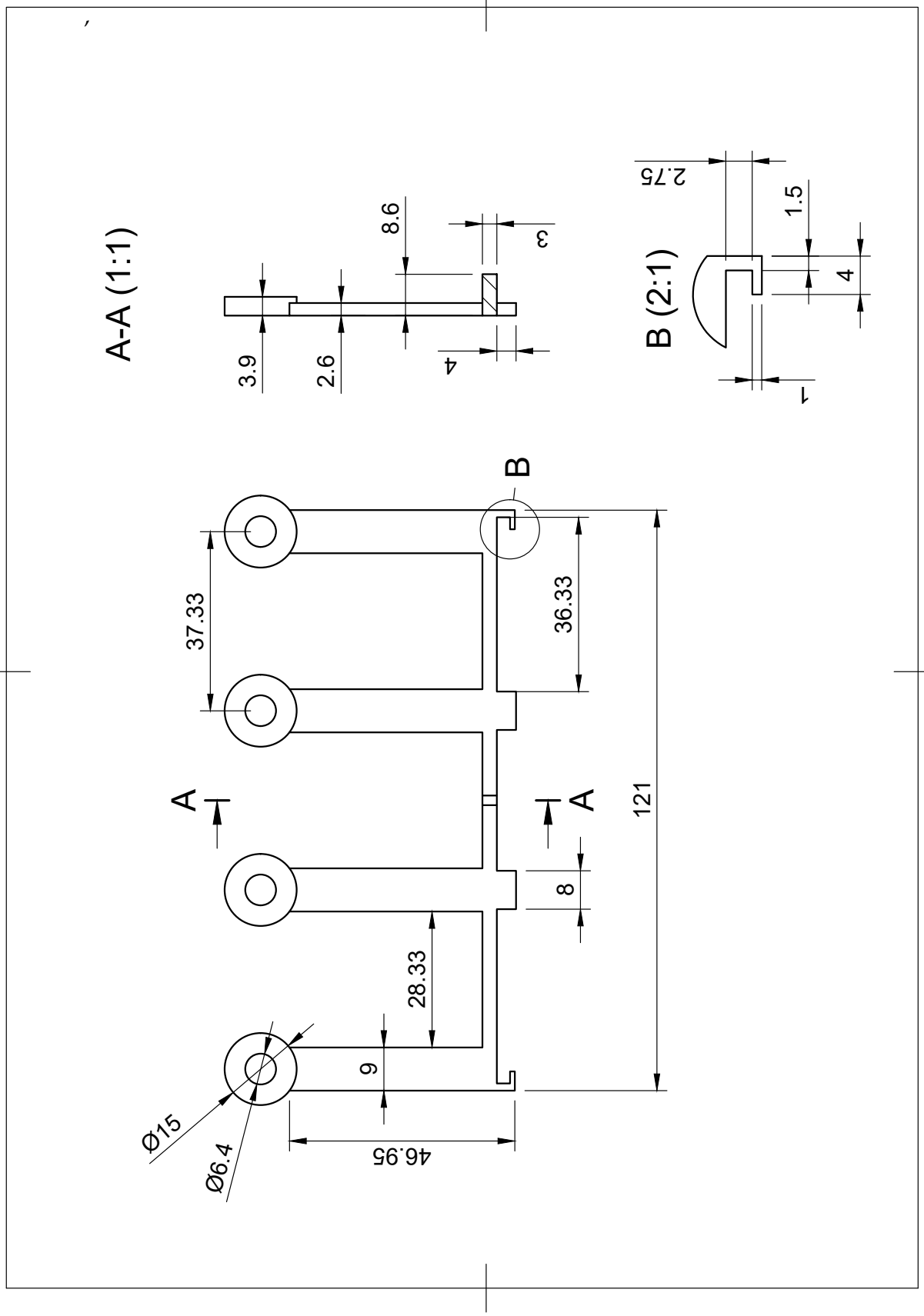

## B.5 Internal grid

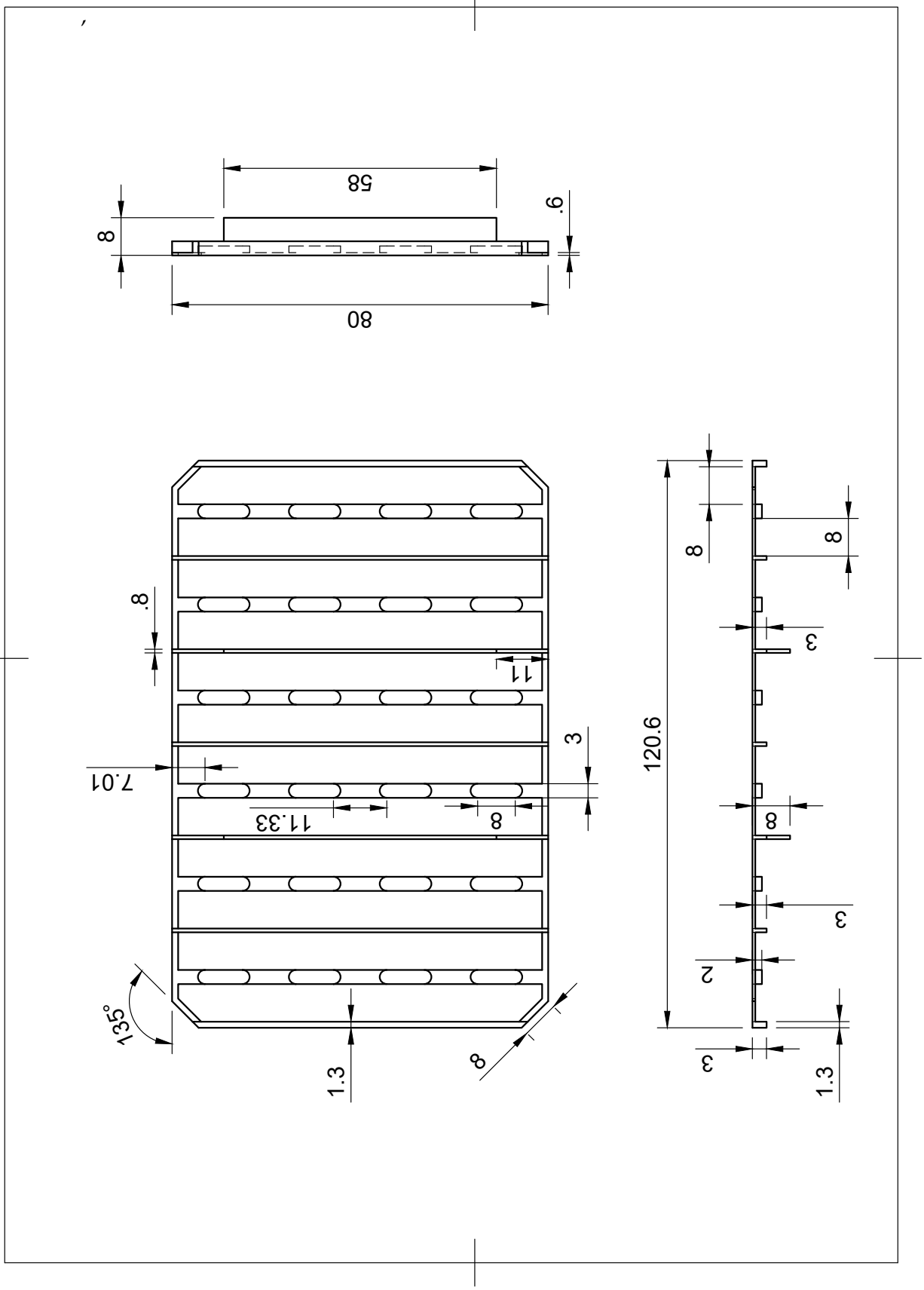

## B.6 Camera support

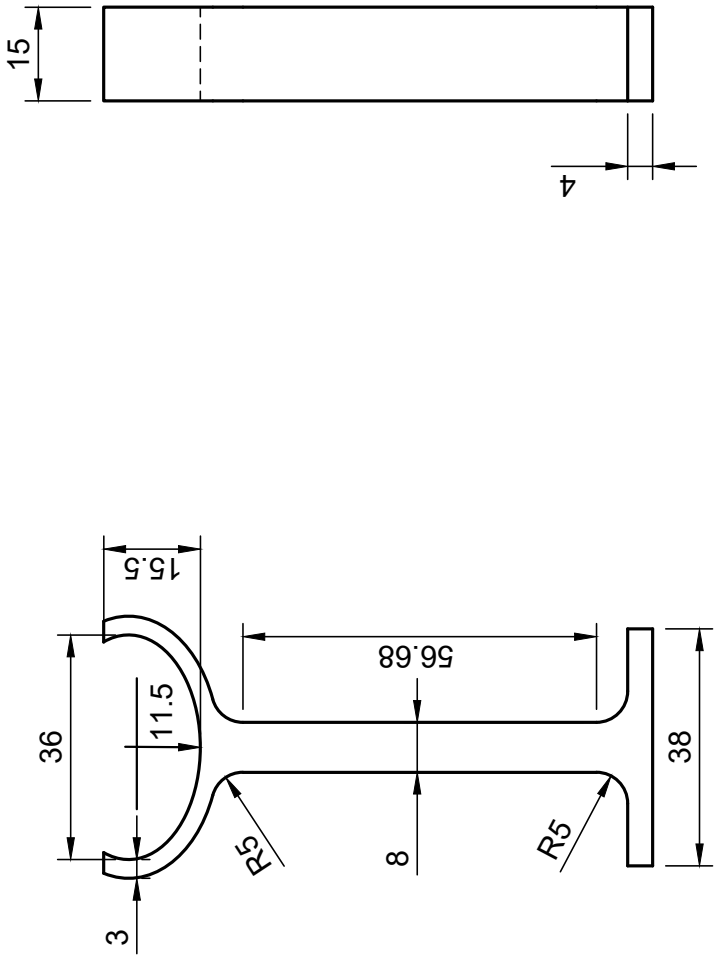

# Bibliography


[1] A. E. Guttmacher, F. S. Collins, and E. G. Nabel, "Genomic medicine cardiovascular disease," *The New England Journal of Medicine*, 2003.

[2] O. Gaidai, Y. Cao, and S. Loginov, "Global cardiovascular diseases death rate prediction," *Current Problems in Cardiology*, vol. 48, 2023.

[3] A. Mathur, Z. Ma, P. Loskill, S. Jeeawoody, and K. E. Healy, "In vitro cardiac tissue models: Current status and future prospects," *Advanced Drug Delivery Reviews*, vol. 96, pp. 203–213, 1 2016.

[4] S. B. Bremner, K. S. Gaffney, N. J. Sniadecki, and D. L. Mack, "A change of heart: Human cardiac tissue engineering as a platform for drug development," 5 2022.

[5] A. Eder, I. Vollert, A. Hansen, and T. Eschenhagen, "Human engineered heart tissue as a model system for drug testing," 1 2016.

[6] P. Camacho, H. Fan, Z. Liu, and J.-Q. He, "Small mammalian animal models of heart disease," 2016.

[7] H. R. Ferdowsian and N. Beck, "Ethical and scientific considerations regarding animal testing and research," *PLoS ONE*, vol. 6, 2011.

[8] I. Jorba, D. Mostert, L. H. Hermans, A. V. D. Pol, N. A. Kurniawan, and C. V. Bouten, "In vitro methods to model cardiac mechanobiology in health and disease," 3 2021.

[9] P. A. Iaizzo, *General features of the cardiovascular system*, pp. 3–12. Springer International Publishing, 1 2015.

[10] R. Chaudhry, A. Rehman, and et al., *Physiology, Cardiovascular*. StatPearls Publishing, 2022.

[11] M. K. Pugsley and R. Tabrizchi, "The vascular system an overview of structure and function," 2000.

[12] P. Sucosky, J. A. Shar, and J. Barrientos, *Cardiovascular mechanics and disease*, pp. 23–45. Elsevier, 2019.

[13] J. D. Humphreyl and A. D. Mcculloch, "The cardiovascular system-anatomy, physiology and cell biology," 2003.

[14] A. F. M. Moorman and V. M. Christoffels, "Cardiac chamber formation: Development, genes, and evolution," *Physiological Reviews*, vol. 83, no. 4, pp. 1223–1267, 2003. PMID: 14506305.

[15] B. J. Gordon, K. A. Young, and J. A. Wise, *Anatomy and Physiology 2e*, ch. 19. openstax, 2021.

[16] R. B. Hinton and K. E. Yutzey, "Heart valve structure and function in development and disease," *Annual Review of Physiology*, vol. 73, pp. 29–46, 2011.

[17] B. R. Berridge, J. F. V. Vleet, and E. Herman, *Cardiovascular System*, pp. 153–194. Elsevier Inc., 2018.

[18] G. M. Fomovsky, S. Thomopoulos, and J. W. Holmes, "Contribution of extracellular matrix to the mechanical properties of the heart," 3 2010.

[19] M. Litviňuková, C. Talavera-López, H. Maatz, D. Reichart, C. L. Worth, E. L. Lindberg, M. Kanda, K. Polanski, M. Heinig, M. Lee, E. R. Nadelmann, K. Roberts, L. Tuck, E. S. Fasouli, D. M. DeLaughter, B. McDonough, H. Wakimoto, J. M. Gorham, S. Samari, K. T. Mahbubani, K. Saeb-Parsy, G. Patone, J. J. Boyle, H. Zhang, H. Zhang, A. Viveiros, G. Y. Oudit, O. A. Bayraktar, J. G. Seidman, C. E. Seidman, M. Noseda, N. Hubner, and S. A. Teichmann, "Cells of the adult human heart," *Nature*, vol. 588, pp. 466–472, 12 2020.

[20] J. Kingma, C. Simard, and B. Drolet, "Overview of cardiac arrhythmias and treatment strategies," *Pharmaceuticals*, vol. 16, no. 6, 2023.

[21] S. Kanno and J. E. Saffitz, "The role of myocardial gap junctions in electrical conduction and arrhythmogenesis," *Cardiovascular Pathology*, vol. 10, no. 4, pp. 169–177, 2001.

[22] E. A. Woodcock and S. J. Matkovich, "Cardiomyocytes structure, function and associated pathologies," 2005.

[23] Y. Ma, L. E. D. C. Brás, H. Toba, R. P. Iyer, M. E. Hall, M. D. Winniford, R. A. Lange, S. C. Tyagi, and M. L. Lindsey, "Myofibroblasts and the extracellular matrix network in post-myocardial infarction cardiac remodeling," 2014.

[24] K. Kimura, M. Ieda, and K. Fukuda, "Development, maturation, and transdifferentiation of cardiac sympathetic nerves," *Circulation Research*, vol. 110, no. 2, pp. 325–336, 2012.

[25] J. W. Calvert and D. J. Lefer, *Overview of Cardiac Muscle Physiology*, vol. 1-2, pp. 57–66. Elsevier, 7 2012.

[26] E. Schmuckk and P. A. Editors, "Cardiac extracellular matrix fundamental science to clinical applications," 2018.

[27] B. Sjögren, C. Bigert, and P. Gustavsson, *Cardiovascular Disease*, vol. 1, pp. 313–331. Elsevier Inc., 2015.

[28] T. Gaziano, K. Reddy, F. Paccaud, at al. Cardiovascular Disease. In: DT Jamison, J. Breman, A. Measham, and at al. editors., *Disease Control Priorities in Developing Countries, Second Edition*, ch. 33, pp. 645–662. Washington (DC): The International Bank for Reconstruction and Development / The World Bank, 2nd ed., July 2006.

[29] R. Shahjehan and B. Bhutta, *Coronary Artery Disease*. In: StatPearls [Internet]. Treasure Island (FL): StatPearls Publishing, January 2023.

[30] L. R. Caplan, R. P. Simon, and S. Hassani, "Chapter 27 - cerebrovascular disease—stroke," in *Neurobiology of Brain Disorders (Second Edition)* (M. J. Zigmond, C. A. Wiley, and M.-F. Chesselet, eds.), pp. 457–476, Academic Press, second edition ed., 2023.

[31] R. R. Sun, M. Liu, L. Lu, Y. Zheng, and P. Zhang, "Congenital heart disease: Causes, diagnosis, symptoms, and treatments," *Cell Biochemistry and Biophysics*, vol. 72, pp. 857–860, 7 2015.

[32] L. Abdurrahman, "Adult congenital heart disease update 12," *Current Problems in Pediatric and Adolescent Health Care*, vol. 53, 3 2023.

[33] R. H. Schwinger, "Pathophysiology of heart failure," 2 2021.

[34] H. Sisakian, "Cardiomyopathies: Evolution of pathogenesis concepts and potential for new therapies," *World Journal of Cardiology*, vol. 6, p. 478, 2014.

[35] H. Saini, S. Tabtabai, J. R. Stone, and P. T. Ellinor, *Pathophysiology of Cardiomyopathies*, pp. 101–119. Elsevier Inc., 2014.

[36] E. M. Alissa and G. A. Ferns, "Heavy metal poisoning and cardiovascular disease," 2011.

[37] J.-E. Tarride, M. Lim, M. DesMeules, W. Luo, N. Burke, D. O'Reilly, J. Bowen, and R. Goeree, "A review of the cost of cardiovascular disease," *Canadian Journal of Cardiology*, vol. 25, no. 6, pp. e195–e202, 2009.

[38] B. Dahlöf, "Cardiovascular disease risk factors: Epidemiology and risk assessment," *The American Journal of Cardiology*, vol. 105, no. 1, Supplement, pp. 3A–9A, 2010. The Cardiovascular Continuum in the 21st Century: Renin-Angiotensin System Blockade.

[39] D. Weycker, G. A. Nichols, M. O'Keeffe-Rosetti, J. Edelsberg, Z. M. Khan, S. Kaura, and G. Oster, "Risk-factor clustering and cardiovascular disease risk in hypertensive patients," *American Journal of Hypertension*, vol. 20, pp. 599–607, 6 2007.

[40] J. W. Twisk, H. C. Kemper, W. Van Mechelen, and G. Post, "Clustering of risk factors for coronary heart disease: The longitudinal relationship with lifestyle," *Annals of Epidemiology*, vol. 11, no. 3, pp. 157–165, 2001.

[41] S. E. Kjeldsen, "Hypertension and cardiovascular risk: General aspects," *Pharmacological Research*, vol. 129, pp. 95–99, 3 2018.

[42] U. J. Tietge, "Hyperlipidemia and cardiovascular disease: Inflammation, dyslipidemia, and atherosclerosis," 2 2014.

[43] C. A. Gleissner, E. Galkina, J. L. Nadler, and K. Ley, "Mechanisms by which diabetes increases cardiovascular disease," *Drug Discovery Today: Disease Mechanisms*, vol. 4, pp. 131–140, 9 2007.

[44] K. C. Zalesin, B. A. Franklin, W. M. Miller, E. D. Peterson, and P. A. McCullough, "Impact of obesity on cardiovascular disease," 9 2008.

[45] A. Banerjee, "A review of family history of cardiovascular disease: Risk factor and research tool," 6 2012.

[46] T. Kondo, Y. Nakano, S. Adachi, and T. Murohara, "Effects of tobacco smoking on cardiovascular disease," 2019.

[47] A. Pan, X. Lin, E. Hemler, and F. B. Hu, "Diet and cardiovascular disease: Advances and challenges in population-based studies," 3 2018.

[48] M. R. Carnethon, "Physical activity and cardiovascular disease: How much is enough?," *American Journal of Lifestyle Medicine*, vol. 3, pp. 44S–49S, 7 2009.

[49] I. R. Whitman, V. Agarwal, G. Nah, J. W. Dukes, E. Vittinghoff, T. A. Dewland, and G. M. Marcus, "Alcohol abuse and cardiac disease," 2017.

[50] T. Esch, G. B. Stefano, G. L. Fricchione, and H. Benson, "Www. medsci monit.com ra stress in cardiovascular diseases," 2002.

[51] J. Egido, C. Zaragoza, C. Gomez-Guerrero, J. L. Martin-Ventura, L. Blanco-Colio, B. Lavin, B. Mallavia, C. Tarin, S. Mas, and A. Ortiz, "Animal models of cardiovascular diseases," 2011.

[52] M. Bader, "Rat models of cardiovascular diseases.," 2010.

[53] T. Jia, C. Wang, Z. Han, X. Wang, M. Ding, and Q. Wang, "Experimental rodent models of cardiovascular diseases," 12 2020.

[54] H. G. Tsang, N. A. Rashdan, C. B. Whitelaw, B. M. Corcoran, K. M. Summers, and V. E. MacRae, "Large animal models of cardiovascular disease," *Cell Biochemistry and Function*, vol. 34, pp. 113–132, 4 2016.

[55] E. M. Walters, E. Wolf, J. J. Whyte, J. Mao, S. Renner, H. Nagashima, E. Kobayashi, J. Zhao, K. D. Wells, J. K. Critser, L. K. Riley, and R. S. Prather, "Completion of the swine genome will simplify the production of swine as a large animal biomedical model," *BMC Medical Genomics*, vol. 5, 2012.

[56] G. Bowley, E. Kugler, R. Wilkinson, A. Lawrie, F. van Eeden, T. J. A. Chico, P. C. Evans, E. S. Noël, and J. Serbanovic-Canic, "Zebrafish as a tractable model of human cardiovascular disease," *British Journal of Pharmacology*, 2022.

[57] S. Lu, M. Hu, Z. Wang, H. Liu, Y. Kou, Z. Lyu, and J. Tian, "Generation and application of the zebrafish heg1 mutant as a cardiovascular disease model," *Biomolecules*, 2020.

[58] L. Drakhlis and R. Zweigerdt, "Heart in a dish - choosing the right in vitro model," *DMM Disease Models and Mechanisms*, vol. 16, 5 2023.

[59] A. K. Kiani, D. Pheby, G. Henehan, R. Brown, P. Sieving, P. Sykora, R. Marks, B. Falsini, N. Capodicasa, S. Miertus, L. Lorusso, D. Dondossola, G. M. Tartaglia, M. C. Ergoren, M. Dundar, S. Michelini, D. Malacarne, G. Bonetti, A. Dautaj, K. Donato, M. C. Medori, T. Beccari, M. Samaja, S. T. Connelly, D. Martin, A. Morresi, A. Bacu, K. L. Herbst, M. Kapustin, L. Stuppia, L. Lumer, G. Farronato, and M. Bertelli, "Ethical considerations regarding animal experimentation," 6 2022.

[60] I. W. Mak, N. Evaniew, and M. Ghert, "Review article lost in translation: animal models and clinical trials in cancer treatment," 2014.

[61] E. Maestri, "The 3rs principle in animal experimentation: A legal review of the state of the art in europe and the case in italy," *BioTech*, vol. 10, 6 2021.

[62] R. C. Hubrecht and E. Carter, "The 3rs and humane experimental technique: Implementing change," *Animals*, vol. 9, 10 2019.

[63] P. C. Asuzu, N. S. Trompeter, C. R. Cooper, S. A. Besong, and A. N. Aryee, "Cell culture-based assessment of toxicity and therapeutics of phytochemical antioxidants," 2 2022.

[64] Y. Liu, Z. Qi, X. Li, Y. Du, and Y. G. Chen, "Monolayer culture of intestinal epithelium sustains lgr5+ intestinal stem cells," 12 2018.

[65] P. F. Egan, "Integrated design approaches for 3d printed tissue scaffolds: Review and outlook," 8 2019.

[66] A. Eltom, G. Zhong, and A. Muhammad, "Scaffold techniques and designs in tissue engineering functions and purposes: A review," 2019.

[67] C. Y. Liaw, S. Ji, and M. Guvendiren, "Engineering 3d hydrogels for personalized in vitro human tissue models," 2 2018.

[68] C. Y. Chang and C. C. Lin, "Hydrogel models with stiffness gradients for interrogating pancreatic cancer cell fate," 3 2021.

[69] Z. Zhao, X. Chen, A. M. Dowbaj, A. Sljukic, K. Bratlie, L. Lin, E. L. S. Fong, G. M. Balachander, Z. Chen, A. Soragni, M. Huch, Y. A. Zeng, Q. Wang, and H. Yu, "Organoids," *Nature Reviews Methods Primers*, vol. 2, 12 2022.

[70] X. Qian, H. Song, and G. L. Ming, "Brain organoids: Advances, applications and challenges," 4 2019.

[71] C. H. Beckwitt, A. M. Clark, S. Wheeler, D. L. Taylor, D. B. Stolz, L. Griffith, and A. Wells, "Liver 'organ on a chip'," 2 2018.

[72] S. Kang, S. E. Park, and D. D. Huh, "Organ-on-a-chip technology for nanoparticle research," 12 2021.

[73] H. Savoji, M. H. Mohammadi, N. Rafatian, M. K. Toroghi, E. Y. Wang, Y. Zhao, A. Korolj, S. Ahadian, and M. Radisic, "Cardiovascular disease models: A game changing paradigm in drug discovery and screening," *Biomaterials*, vol. 198, pp. 3–26, 4 2019.

[74] G. Abdelsayed, D. Ali, A. Malone, J. Saidi, M. Myneni, K. Rajagopal, F. H. Cheema, and A. Hameed, "2d and 3d in-vitro models for mimicking cardiac physiology," *Applications in Engineering Science*, vol. 12, 12 2022.

[75] C. C. Kartha, *Response of Cardiomyocytes to Mechanical Stress*, pp. 95–114. Cham: Springer International Publishing, 2021.

[76] E. Ovchinnikova, M. Hoes, K. Ustyantsev, N. Bomer, T. V. de Jong, H. van der Mei, E. Berezikov, and P. van der Meer, "Modeling human cardiac hypertrophy in stem cell-derived cardiomyocytes," *Stem Cell Reports*, vol. 10, pp. 794–807, 3 2018.

[77] A. Hansen, A. Eder, M. Bönstrup, M. Flato, M. Mewe, S. Schaaf, B. Aksehirlioglu, A. Schwörer, J. Uebeler, and T. Eschenhagen, "Development of a drug screening platform based on engineered heart tissue," *Circulation Research*, vol. 107, pp. 35–44, 7 2010.

[78] X. Wang, M. Jiang, Z. Zhou, J. Gou, and D. Hui, "3d printing of polymer matrix composites: A review and prospective," *Composites Part B: Engineering*, vol. 110, pp. 442–458, 2 2017.

[79] F. M. Mwema and E. T. Akinlabi, *Basics of Fused Deposition Modelling (FDM)*, pp. 1–15. Springer, 2020.

[80] A. Jandyal, I. Chaturvedi, I. Wazir, A. Raina, and M. I. U. Haq, "3d printing – a review of processes, materials and applications in industry 4.0," *Sustainable Operations and Computers*, vol. 3, pp. 33–42, 1 2022.

[81] Autodesk, *Fusion 360*. 2023.

[82] Raise3D, *IdeaMaker*. 2023.

[83] I. J. Solomon, P. Sevvel, and J. Gunasekaran, "A review on the various processing parameters in fdm," *Materials Today: Proceedings*, vol. 37, pp. 509–514, 2021. International Conference on Newer Trends and Innovation in Mechanical Engineering: Materials Science.

[84] E. H. Tümer and H. Y. Erbil, "Extrusion-based 3d printing applications of pla composites: A review," *Coatings*, vol. 11, no. 4, 2021.

[85] Y. Yang, L. Zhang, Z. Xiong, Z. Tang, R. Zhang, and J. Zhu, "Research progress in the heat resistance, toughening and filling modification of pla," 11 2016.

[86] M. T. Mubarak, I. Ozsahin, and D. U. Ozsahin, "Evaluation of sterilization methods for medical devices," 2019.

[87] MathWorks, *MATLAB*. 2023.

[88] S. Schaaf, A. Eder, I. Vollert, A. Stöhr, A. Hansen, and T. Eschenhagen, "Generation of strip-format fibrin-based engineered heart tissue (eht)," *Methods in Molecular Biology*, vol. 1181, pp. 121–129, 2014.

[89] Z. Cao, Y. Jia, and B. Zhu, "Bnp and nt-probnp as diagnostic biomarkers for cardiac dysfunction in both clinical and forensic medicine," 4 2019.

[90] C. Hall, "Essential biochemistry and physiology of (nt-pro)bnp," 3 2004.

[91] M. Weber and C. Hamm, "Role of b-type natriuretic peptide (bnp) and nt-probnp in clinical routine," 6 2006.

[92] A. D. Castelnuovo, G. Veronesi, S. Costanzo, T. Zeller, R. B. Schnabel, A. D. Curtis, V. Salomaa, R. Borchini, M. Ferrario, S. Giampaoli, F. Kee, S. Söderberg, T. Niiranen, K. Kuulasmaa, G. D. Gaetano, M. B. Donati, S. Blankenberg, and L. Iacoviello, "Nt-probnp (n-terminal pro-b-type natriuretic peptide) and the risk of stroke: Results from the biomarcare consortium," *Stroke*, vol. 50, pp. 610–617, 3 2019.

[93] O. A. Goryacheva, T. D. Ponomaryova, D. D. Drozd, A. A. Kokorina, T. Y. Rusanova, P. K. Mishra, and I. Y. Goryacheva, "Heart failure biomarkers bnp and nt-probnp detection using optical labels," 1 2022.

[94] S. Sharma, P. G. Jackson, and J. Makan, "Cardiac troponins," 10 2004.

[95] T. Wakabayashi and S. Ebashi, "Troponin," 2004.

[96] L. C. Duque-Ossa, B. García-Ferrera, and J. A. Reyes-Retana, "Troponin i as a biomarker for early detection of acute myocardial infarction," 5 2023.

[97] J. A. D. Lemos, "Increasingly sensitive assays for cardiac troponins a review," 2013.

[98] J. M. Bliley, M. C. S. C. Vermeer, R. M. Duffy, I. Batalov, D. Kramer, J. W. Tashman, D. J. Shiwarski, A. Lee, A. S. Teplenin, L. Volkers, B. Coffin, M. F. Hoes, A. Kalmykov, R. N. Palchesko, Y. Sun, J. D. H. Jongbloed, N. Bomer, R. A. de Boer, A. J. H. Suurmeijer, D. A. Pijnappels, M. C. Bolling, P. van der Meer, and A. W. Feinberg, "Dynamic loading of human engineered heart tissue enhances contractile function and drives a desmosome-linked disease phenotype," *Sci. Transl. Med*, vol. 13, p. 1817, 2021.

[99] J. Guo and N. Huebsch, "Modeling the response of heart muscle to mechanical stimulation in vitro," *Current Tissue Microenvironment Reports*, vol. 1, pp. 61–72, 9 2020.

[100] K. G. Shyu, "Cellular and molecular effects of mechanical stretch on vascular cells and cardiac myocytes," 3 2009.

[101] H. Kurazumi, M. Kubo, M. Ohshima, Y. Yamamoto, Y. Takemoto, R. Suzuki, S. Ikenaga, A. Mikamo, K. Udo, K. Hamano, and T. S. Li, "The effects of mechanical stress on the growth, differentiation, and paracrine factor production of cardiac stem cells," *PLoS ONE*, vol. 6, 12 2011.

[102] B. R. Weil, G. Suzuki, R. F. Young, V. Iyer, and J. M. Canty, "Troponin release and reversible left ventricular dysfunction after transient pressure overload," *Journal of the American College of Cardiology*, vol. 71, pp. 2906–2916, 6 2018.

[103] S. R. Gu, Y. G. Kang, J. W. Shin, and J. W. Shin, "Simultaneous engagement of mechanical stretching and surface pattern promotes cardiomyogenic differentiation of human mesenchymal stem cells," *Journal of Bioscience and Bioengineering*, vol. 123, pp. 252–258, 2 2017.